1 **Nitrate Chemistry in the Northeast US Part II: Oxygen Isotopes Reveal**

2 **Differences in Particulate and Gas Phase Formation**

3 Heejeong Kim[1,2*], Wendell W. Walters[2*], Claire Bekker[1, a], Lee T. Murray[3], and Meredith G.

4 Hastings[1,2]

5 [1]Department of Earth, Environmental, and Planetary Sciences, Brown University; Providence, RI 02912, USA.

6 [2]Institute at Brown for Environment and Society, Brown University; Providence, RI 02912, USA

7 [3]Department of Earth and Environmental Sciences, University of Rochester; Rochester, NY 14627, USA

8 [a]Now at Environmental Health Sciences, University of California Los Angeles; Los Angeles, CA 90095

10 *Correspondence to*:

11 Heejeong Kim (heejeong_kim@brown.edu)

12 Wendell W. Walters (wendell_walters@brown.edu)

14 **Abstract.** The northeastern US represents a mostly urban corridor impacted by high population

15 and fossil-fuel combustion emission density. This has led to historically degraded air quality and

16 acid rain that has been a focus of regulatory-driven emissions reductions. Detailing the chemistry

17 of atmospheric nitrate formation is critical for improving the model representation of atmospheric

18 chemistry and air quality. The oxygen isotopic composition of atmospheric nitrate are useful

19 indicators in tracking nitrate formation pathways. Here, we measured oxygen isotope deltas ($\Delta(^{17}O)$

20 and $\delta(^{18}O)$) for nitric acid (HNO_3) and particulate nitrate (pNO_3) from three US EPA Clean Air

21 Status and Trends Network (CASTNET) sites in the northeastern US from December 2016 to 2018.

22 The $\Delta(^{17}O, HNO_3)$ and $\delta(^{18}O, HNO_3)$ values ranged from 12.9 ‰ to 30.9 ‰ and from 46.9 ‰ to

23 82.1 ‰, and the $\Delta(^{17}O, pNO_3)$ and $\delta(^{18}O, pNO_3)$ ranged from 16.6 ‰ to 33.7 ‰ and from 43.6 ‰

24 to 85.3 ‰, respectively. There was distinct seasonality of $\delta(^{18}O)$ and $\Delta(^{17}O)$ with higher values

25 observed during winter compared to summer, suggesting a shift in O_3 to HO_x radical chemistry, as

26 expected. Unexpectedly, there was a statistical difference in $\Delta(^{17}O)$ between HNO_3 and pNO_3, with

27   higher values observed for pNO$_3$ (27.1±3.8) ‰ relative to HNO$_3$ (22.7±3.6) ‰, and significant

28   differences in the relationship between $\delta(^{18}O)$ and $\Delta(^{17}O)$. This difference suggests atmospheric

29   nitrate phase-dependent oxidation chemistry that is not predicted in models. Based on the output

30   from GEOS-Chem, and both the $\delta(^{18}O)$ and $\Delta(^{17}O)$ observations, we quantify the production

31   pathways of atmospheric nitrate. The model significantly overestimated the heterogeneous N$_2$O$_5$

32   hydrolysis production for both HNO$_3$ and pNO$_3$, a finding consistent with observed seasonal

33   changes in $\delta(^{18}O)$ and $\Delta(^{17}O)$ of HNO$_3$ and pNO$_3$, though large uncertainties remain in the

34   quantitative transfer of $\delta(^{18}O)$ from major atmospheric oxidants. This comparison provides

35   important insight into the role of oxidation chemistry in reconciling a commonly observed positive

36   bias for modeled atmospheric nitrate concentrations in the northeastern US.

1. Introduction

39   Nitrogen oxides (NO$_x$ = NO + NO$_2$) in the atmosphere have an important impact on air quality and

40   human and ecosystem health (Galloway et al., 2004). NO$_x$ plays an important role in influencing

41   the oxidizing efficiency of the atmosphere, including the production of ozone (O$_3$), and leads to

42   the formation of atmospheric nitrate (gas phase nitric acid (HNO$_3$) and nitrate in particulate form

43   (pNO$_3$)) (Crutzen et al., 1979). HNO$_3$ and pNO$_3$ are, in turn, important contributors to dry and wet

44   N deposition. Nitrate is a key component of particulate matter (PM$_{2.5}$), which has direct adverse

45   effects on human respiratory and climate change, and the deposition of N to ecosystems can

46   contribute to soil acidification and eutrophication (Camargo and Alonso, 2006; Schlesinger, 2007;

47   Tai et al., 2010). Thus, changes in the chemistry and chemical feedbacks associated with NO$_x$ have

48   important implications for predicting air quality improvements and climatic responses.

49

50   The US Environmental Protection Agency (EPA) reported that NO$_x$ emissions have decreased by

51   36 % in the United States from 2007 to 2015 due to effective regulations in response to the Clean

52   Air Act and its Amendments (US EPA, 2017; CASTNET, 2019; NEI, 2017; Shah et al., 2018).

53   However, atmospheric pNO$_3$ concentrations have responded sub-linearly to the dramatic NO$_x$

54   emission reductions, with only a 7.8 % pNO$_3$ decrease over the same period in the northeastern

55   US. Uncertainties in our understanding between NO$_x$ reductions and the production of atmospheric

56   nitrate challenge our ability to make effective reductions in reactive nitrogen concentrations. Major

57   factors influencing atmospheric nitrate production include oxidant availability, heterogeneous

58 chemistry, gas-to-particle partitioning, and potential aerosol nitrate photolysis (Jaeglé et al., 2018;

59 Shah et al., 2018; Kasibhatla et al., 2018).

60

61 Atmospheric nitrate concentrations have been simulated using various chemistry models to detail

62 spatiotemporal variabilities between precursor NO_x emissions and nitrate in the US, with

63 somewhat limited success (Walker et al., 2012; Zhang et al., 2012). In particular, the

64 concentrations of nitrate observed in the northeastern US tend to be overestimated in models (e.g.,

65 Heald et al., 2012; Zhang et al., 2012), which is an important region to monitor due to its high

66 population density, transport patterns and the tendency for poor air quality (Sickles and Shadwick,

67 2015). Modeling studies suggest that biases revealed by comparison with observations could be

68 due to uncertainties in NO_x and gaseous ammonia (NH_3) emission estimates, dry deposition

69 removal rates, heterogeneous chemical production rates, and changing chemistry due to reductions

70 in NO_x and sulfur dioxide emissions (Heald et al., 2012; Holt et al., 2015; Shah et al., 2018).

71

72 The nitrate oxygen isotope deltas ($\Delta(^{17}O)$ and $\delta(^{18}O)$) have proven to provide observational

73 constraints on the oxidation pathways that are responsible for the formation of atmospheric nitrate

74 (Hastings et al., 2003; Michalski et al., 2003; Alexander et al., 2009). The isotopic composition is

75 expressed as δ, which is a standardized notation and quantified as $\delta = (R_{sample}/R_{reference} - 1)$. R is

76 the ratio of the heavy isotope to the light isotope (e.g., $^{18}O/^{16}O$; $^{17}O/^{16}O$) in the sample and

77 internationally recognized isotopic reference material (Vienna Standard Mean Ocean Water),

78 respectively. Several studies have suggested that the distinctive ($\Delta(^{17}O) = \delta(^{17}O) - 0.52 \times \delta(^{18}O)$)

79 and $\delta(^{18}O)$ signatures of atmospheric oxidants such as O_3, $O_2/RO_2/HO_2$, H_2O and OH are

80 incorporated into nitrate, tracking the oxidation chemistry of NO_x (Hastings et al., 2003; Michalski

81 et al., 2003; Savarino et al., 2007). Traditionally, the influence of O_3 incorporation in nitrate has

82 been quantitively tracked using only $\Delta(^{17}O)$, because of the unique mass-independent fractionation

83 that results in O_3 carrying excess $\delta(^{17}O)$, yielding a transferrable $\Delta(^{17}O) = (39\pm2)$ ‰ (Thiemens,

84 2006; Vicars and Savarino, 2014). However, all other atmospheric oxidants contain expected

85 mass-dependent signatures such that all have $\Delta(^{17}O)$ value of approximately 0 ‰. The $\delta(^{18}O)$ of

86 atmospheric oxidants could provide further insights into nitrate production mechanisms, especially

87 in cases where oxidants other than O_3 are important, since it is distinctive for each oxidant (e.g.,

88 $\delta(^{18}O, O_3) = (126.3\pm12)$ ‰, $\delta(^{18}O, O_2) = 23$ ‰, $\delta(^{18}O, OH) = -43$ ‰ (Michalski et al., 2012; Vicars

89 and Savarino, 2014)).

90

91 The northeastern US remains an important region to monitor due to historically degraded air

92 quality by NO_x emissions and negative atmospheric nitrate deposition impacts on sensitive

93 ecosystems. Changes in oxidation chemistry and chemical feedbacks associated with nitrate

94 production and deposition have important implications for predicting air quality improvements

95 and informing policy recommendations. In this study, using the Clean Air Status and Trends

96 Network (CASTNET) samples, we explored spatiotemporal differences in HNO_3 and pNO_3

97 concentrations and production mechanisms in the northeastern US over two years. Based on these

98 observations, we aimed to better constrain the mismatch in modeled predictions of atmospheric

99 nitrate chemistry in the northeastern US. This is the first study to quantitatively evaluate the triple

100 oxygen isotope composition from observations and model simulations in the northeastern US. The

101 comparison with the combination of $\Delta(^{17}O)$ and $\delta(^{18}O)$ values, and both gaseous and particle

102 phases of nitrate, provide a significant advance in our ability to probe the representation of

103 oxidation chemistry in atmospheric chemistry models.

104

105

106 **2. Methods**

107 **2.1 CASTNET Samples**

108 Atmospheric nitrate samples were collected by the US EPA at several locations of Clean Air Status

109 and Trends Network (CASTNET) sites in the northeastern US (**Figure 1**). Three CASTNET sites

110 were selected: Abington, CT (ABT147, 41.84° N, -72.01° W), Connecticut Hill, NY (CTH110,

111 42.40° N, -76.65° W), Woodstock, NH (WST109, 43.94° N, -71.70° W). The samples were

112 collected weekly from December 23, 2016, to December 28, 2018, using a three-stage filter pack

113 system. Based on EPA protocols, pNO_3 was collected using a Teflon filter in the first stage of the

114 filter pack, and gaseous HNO_3 was collected using a Nylon filter in the second stage of the filter

115 pack. We note that due to the semi-volatile characteristic of ammonium nitrate, some pNO_3 might

116 volatilize as HNO_3 and collect downstream of the filter pack leading to negative biases for pNO_3

117 and positive biases for HNO_3 collection (Hering and Cass, 1999; Ashbaugh and Eldred, 2004).

118

119   **2.2 Concentration and Isotope Analyses**

120   Filters were extracted and measured for nitrate concentration using Ion Chromatography and then

121   stored in the CASTNET laboratory at room temperature for up to two years. Extracted samples

122   were shipped to Brown University in the summer of 2020. Nitrate concentrations were measured

123   at Brown University to check for stability of nitrate using standard colorimetric methods (i.e., US

124   EPA Method 353.2) on an automated discrete UV-Vis Analyzer (SmartChem Westco Scientific

125   Instruments, Inc.). The limit of detection was 0.1 and 0.3 μM for nitrite and nitrate, respectively,

126   and the pooled standard deviation of replicate quality control standards was better than 3 %.

127   Overall, strong positive correlations were found between measured concentrations at Brown and

128   reported CASTNET data for both HNO_3 ($y = 0.99x - 0.08$ ($R^2 = 0.99$); $p < 0.05$) and pNO_3 ($y =$

129    $1.04x + 0.09$ ($R^2 = 0.99$); $p < 0.05$) (**Figure 2**); we, therefore, consider the samples representative

130   of their original concentrations.

131

132   The samples were collected once a week, and equal volumes of filter extract were combined for

133   isotope analysis to produce monthly aggregates for HNO_3 and pNO_3, respectively. Oxygen ($\delta(^{18}O)$

134   and $\Delta(^{17}O)$) stable isotopic compositions in HNO_3 and pNO_3 were analyzed utilizing the bacterial

135   denitrifier method at Brown University (Sigman et al., 2001; Casciotti et al., 2002; Kaiser et al.,

136   2007). Briefly, samples were injected into a buffer solution containing *P. aureofaciens,* which lack

137   the nitrous oxide (N_2O) reductase enzyme, and sample nitrate was quantitatively reduced to N_2O.

138   For $\delta(^{18}O)$ analysis, the generated N_2O is injected into a Thermo-Finnegan Delta V Plus isotope

139   ratio mass spectrometry (IRMS) with a modified Gas Bench system after flowing through an

140   automated extraction and purification system. Determination of $\delta(^{18}O)$ in N_2O was conducted at

141   an *m/z* of 44, 45, and 46 and corrected using internationally recognized isotopic reference materials

142   that included IAEA-NO_3 (25.6 ‰), USGS34 (-27.9 ‰), and USGS35 (57.5 ‰). The $\Delta(^{17}O)$ was

143   determined in a separate analysis. The bacteria-generated N_2O was decomposed to N_2 and O_2 in a

144   gold furnace heated to 770 ºC and analyzed at *m/z* 32, 33, and 34 to determine $^{17}O/^{16}O$ and $^{18}O/^{16}O$

145   ratios of the evolved O_2. The 33/32 and 34/32 mass ratios were corrected using isotopic reference

146   materials, USGS34 (-0.29 ‰) and USGS35 (21.6 ‰), and then $\Delta(^{17}O)$ was determined from $\Delta(^{17}O)$

147    $= \delta(^{17}O) - 0.52 \times \delta(^{18}O)$. Due to sample mass limitations, some samples were only analyzed for

148    $\delta(^{18}O)$. The number of samples that were not measured for $\Delta(^{17}O)$ was 1 HNO_3 sample from

149   CTH110, 2 HNO_3 samples from ABT147, 5 pNO_3 samples from CTH110, and 16 pNO_3 samples

150 from WST109. The overall pooled standard deviations of isotopic reference materials and sample

151 numbers were as followed: USGS34 ($\sigma(\delta(^{18}O))$ = 0.5 ‰ (n = 21); $\sigma(\Delta(^{17}O))$ = 1 ‰ (n = 26));

152 USGS35 ($\sigma(\delta(^{18}O))$ = 0.4 ‰ (n = 27); $\sigma(\Delta(^{17}O))$ = 2 ‰ (n = 26)), and IAEA-N3 ($\sigma(\delta(^{18}O))$ = 0.3

153 ‰ (n = 23)).

154

155 **2.3 GEOS-Chem Modeling**

156 The GEOS-Chem global model of atmospheric chemistry (Bey et al., 2001; Walker et al., 2012;

157 2019) was utilized to track the production of NO_2 and HNO_3 at the CASTNET sites and further to

158 model the oxygen isotope deltas (e.g., $\delta(^{18}O)$ and $\Delta(^{17}O)$) following a previous framework

159 (Alexander et al., 2020). Following this framework, oxidation chemistry is tagged only for HNO_3

160 production and is assumed to be the same for pNO_3. We use version 13.2.1

161 (doi:10.5281/zenodo.5500717) of the model driven by GEOS5-FP assimilated meteorology from

162 the NASA Global Modeling and Assimilation Office (GMAO). A nested grid (0.25° latitude ×

163 0.3125° longitude horizontal resolution; ~25 km) simulation was conducted over the northeastern

164 United States (97°-60° W; 35°-60º N) in 2017 and 2018. Boundary conditions were from global

165 simulations performed at 4° latitude × 5° longitude horizontal resolution for the same years after

166 a one-year initialization. Gas- and aerosol-phase chemistry was simulated using the default

167 "fullchem" mechanism (Bates and Jacob, 2019; Wang et al., 2021). Inorganic gas and aerosol

168 partitioning were conducted using version 2.2 of the ISORROPIA II thermodynamic equilibrium

169 model (Fountoukis and Nenes, 2007).

170

171 All default anthropogenic emissions were applied, which is primarily version 2.0 of the

172 Community Emissions Data System (Hoesly et al., 2018) as implemented by McDuffie et al.

173 (2020). Natural emissions respond to local meteorology and include biogenic VOCs from

174 terrestrial plants and the ocean (Millet et al., 2010; Guenther et al., 2012; Hu et al., 2015; Breider

175 et al., 2017), NO_x from lightning and soil microbial activity (Murray et al., 2012; Hudman et al.,

176 2012), mineral dust (Ridley et al., 2012), and sea salt (Jaeglé et al., 2011; Huang and Jaeglé, 2017).

177 Biomass burning emissions were monthly means from version 4.1s of the Global Fire Emissions

178 Database (GFED4.1s; van der Werf et al., 2017). Wet deposition for water-soluble aerosols is

179 described by Liu et al. (2001) and by Amos et al. (2012) for gases. Dry deposition is based on the

180 resistance-in-series scheme of Wesely (1989). Diagnostics were implemented to archive the total

181 production and loss pathways of NO_y, NO_x, NO_2, $RONO_2$, HNO_3 and pNO_3, including the net flux

182 of mass between HNO_3 and pNO_3 in ISOROPPIA II. We evaluated model performance for

183 simulating concentrations and isotope deltas ($\delta(^{18}O)$ and $\Delta(^{17}O)$) using the Normalized Mean Bias

184 (B) metric (Eq.1):

185 $B = (\sum (\bar{Q}_m - \bar{Q}_o) / \sum \bar{Q}_o)$ (Eq.1)

186 where $\bar{Q}_m$ = modeled quantities and $\bar{Q}_o$ = observed quantities.

187

188 **2.4 $\delta(^{18}O)$ and $\Delta(^{17}O)$ Calculations Based on Model Outputs**

189 The oxygen isotope deltas ($\delta(^{18}O)$ and $\Delta(^{17}O)$) of nitrate were calculated based on oxygen isotope

190 mass-balance using production rate outputs from the GEOS-Chem global 3-D model and

191 compared with our observations. Expected $\delta(^{18}O)$ and $\Delta(^{17}O)$ ranges resulting from nitrate

192 production pathways have been previously described and calculated using oxygen mass-balance

193 (Alexander et al., 2009, 2020; Michalski et al., 2003; Morin et al., 2011; Carter et al., 2021). Briefly,

194 the $\delta(^{18}O)$ and $\Delta(^{17}O)$ of nitrate are determined by both NO_x photochemical cycling and nitrate

195 formation reactions (Alexander et al., 2009; Walters et al., 2018). During NO_x photochemical

196 cycling, the oxygen isotopic compositions of NO_x are determined by the relative production rates

197 of NO_2 via reaction of NO with O_3, peroxy and hydroperoxyl radicals, and halogen oxides (XO;

198 BrO, ClO). The proportional contribution of O_3 during NO oxidation is denoted as A and is

199 calculated using

200

201 $A = (k(O_3+NO) [O_3] + k(XO+NO)[XO])/(k(O_3+NO)[O_3] + k(XO+NO)[XO] + k(HO_2+NO)[HO_2]$

202 $+ k(RO_2+NO)[RO_2])$ (Eq. 2)

203

204 where k is the respective rate constant for NO oxidation via O_3, XO, HO_2, and RO_2. The $\Delta(^{17}O)$

205 value of the terminal oxygen atom in O_3 (O_3^*) is assumed to be (39±2) ‰ based on observations,

206 while all other oxidants are assumed to be 0 ‰ (Vicars et al., 2012; Vicars and Savarino, 2014;

207 Alexander et al., 2020). $\delta(^{18}O)$ and $\Delta(^{17}O)$ values of nitrate from each production pathway were

208 then determined using O mass-balance based on the O transfer from varying oxidants involved in

209 its formation (**Table 1**).

210

211   The GEOS-Chem global model has been previously used to quantify nitrate production pathways
212   based on $\Delta(^{17}O)$ (Alexander et al., 2009, 2020), but this has not been done for $\delta(^{18}O)$. Using a
213   similar framework as for $\Delta(^{17}O)$, we expect that $\delta(^{18}O)$ of NO_2 reflects isotopic signatures of both
214   O_3 and O_2, as it has been assumed that the O isotopic composition of RO_2 and HO_2 is equal to O_2
215   (Michalski et al, 2012; Walters et al., 2018). Accordingly, the values of $\delta(^{18}O, NO_2)$ can be
216   predicted by the proportional contribution of O_3 and both HO_2 and RO_2 during NO_x cycling with
217   their distinct $\delta(^{18}O)$ values of O_3 and O_2 (Eq. 3; **Table 1**).

218

219   $\delta(^{18}O, NO_2) = A(\delta(^{18}O, O_3{}^*)) + (1\text{-}A)(\delta(^{18}O, O_2))$ (Eq.3)

220

221   The $\delta(^{18}O)$ values of O_3 and O_2 are adopted from previous studies that determined $\delta(^{18}O, O_3{}^*)$ and
222   $\delta(^{18}O, O_2)$ as 126.3 ‰ and 23 ‰ (Vicars and Savarino, 2014; Kroopnick and Craig, 1972,
223   respectively). For the calculation of $\delta(^{18}O)$ of nitrate, the value of $\delta(^{18}O)$ of $H_2O(l)$ is assumed to
224   be -6 ‰, which is a typical mid-latitude value and represents water in the liquid phase incorporated
225   into nitrate formation associated with heterogeneous reactions by N_2O_5 or NO_2 hydrolysis
226   (Michalski et al, 2012). The $\delta(^{18}O)$ value of OH can be dependent on both O_3 and $H_2O(g)$, as well
227   as environmental conditions since oxygen in OH can exchange with $H_2O(g)$ (Dubey et al. 1997).
228   Fractionation factors associated with the O transfer into NO_y products are unknown and therefore
229   were not considered. The $\delta(^{18}O)$ of $H_2O(g)$ was estimated based on the equilibrium between $H_2O(l)$
230   and $H_2O(g)$ with a temperature-dependent fractionation factor (1.0094 at 298K); it is assumed that
231   OH and $H_2O(g)$ exist in isotopic equilibrium, which has a theoretically determined fractionation
232   factor (1.0371 at 298K) and leads to an estimate of $\delta(^{18}O, OH)$ of -43 ‰ (Michalski et al, 2012;
233   Walters and Michalski, 2016). We note that the typical annual temperature for the northeast US is
234   approximately 287 K, yielding a $\delta(^{18}O, OH)$ of -45 ‰; for comparison purposes with prior
235   publications, we utilize -43 ‰, which makes little difference in the quantitative results below. In
236   the final step, $\delta(^{18}O)$ or $\Delta(^{17}O)$ of total atmospheric nitrate were calculated based on the monthly-
237   averaged production rates from GEOS-Chem and the seven major reactions that produce nitrate in
238   the model (**Table 1**) to compare with observations.

239

240

241   **3. Results and Discussion**

242   ### 3.1 Spatiotemporal Variations of Atmospheric Nitrate Concentration

243

244   **Figure 3** shows the monthly averaged spatiotemporal variations of HNO_3 and pNO_3 mass

245   concentration (denoted as γ). The observed (o) HNO_3 concentrations ($\gamma_o(HNO_3)$) ranged from 0.11

246    $\mu g\ m^{-3}$ to 0.88 $\mu g\ m^{-3}$, with a mean value of 0.46 $\mu g\ m^{-3}$ across the three CASTNET sites. The

247   observed pNO_3 concentrations ($\gamma_o(pNO_3)$) ranged from 0.04 $\mu g\ m^{-3}$ to 2.01 $\mu g\ m^{-3}$, with a mean

248   value of 0.50 $\mu g\ m^{-3}$, and showed clear seasonality at all three sites with averaged higher values

249    $(0.75\pm0.52)\ \mu g\ m^{-3}$ in the cold season (October to March) and lower values $(0.25\pm0.17)\ \mu g\ m^{-3}$ in

250   the warm season (April to September), which were significantly different ($p < 0.01$). On the other

251   hand, $\gamma_o(HNO_3)$ was seasonally invariable with $(0.42\pm0.17)\ \mu g\ m^{-3}$ for cold season and (0.50 ± 0.24)

252    $\mu g\ m^{-3}$ for warm season that was not statistically different ($p > 0.05$). Averaged $\gamma_o(HNO_3)$ was

253   generally lower than pNO_3 across the sites, but the difference was statistically insignificant ($p >$

254   0.05). Both $\gamma_o(HNO_3)$ and $\gamma_o(pNO_3)$ indicated spatial variability with higher values at ABT147 and

255   CTH110 than the WST109 site. The mean annual $\gamma_o(HNO_3)$ and $\gamma_o(pNO_3)$ were $(0.61\pm0.15)\ \mu g\ m^{-3}$

256   and $(0.66\pm0.34)\ \mu g\ m^{-3}$ at ABT147, $(0.55\pm0.13)\ \mu g\ m^{-3}$ and $(0.68\pm0.58)\ \mu g\ m^{-3}$ at CTH110, and

257    $(0.22\pm0.06)\ \mu g\ m^{-3}$ and $(0.17\pm0.13)\ \mu g\ m^{-3}$ at WST109, respectively.

258

259   The modeled (m) HNO_3 concentrations ($\gamma_m(HNO_3)$) ranged from 0.20 $\mu g\ m^{-3}$ to 2.36 $\mu g\ m^{-3}$, with

260   a mean value of 0.82 $\mu g\ m^{-3}$ and modeled pNO_3 concentrations ($\gamma_m(pNO_3)$) ranged from 0.20 μg

261   m^{-3} to 5.27 $\mu g\ m^{-3}$, with a mean value of 1.89 $\mu g\ m^{-3}$. Contrary to our observed data, no consistent

262   spatial variability was observed for $\gamma_m(HNO_3)$ and $\gamma_m(pNO_3)$. The mean $\gamma_m(HNO_3)$ and $\gamma_m(pNO_3)$

263   were $(1.09\pm0.62)\ \mu g\ m^{-3}$ and $(1.73\pm1.13)\ \mu g\ m^{-3}$ at ABT147, $(0.74\pm0.46)\ \mu g\ m^{-3}$ and (2.42 ± 1.71)

264    $\mu g\ m^{-3}$ at CTH110, and $(0.64\pm0.22)\ \mu g\ m^{-3}$ and $(1.52\pm1.24)\ \mu g\ m^{-3}$ at WST109, respectively.

265   However, there are significant seasonal model biases for the HNO_3 and pNO_3. The model

266   significantly overestimates pNO_3 during the winter (3-9 times) and overestimates HNO_3 during

267   the summer (2-3 times).

268

269   As stated above, there can be negative biases for pNO_3 and positive biases for HNO_3 collection,

270   but these should be reduced by comparing the model to total atmospheric nitrate ($tNO_3 = HNO_3 +$

271   pNO_3). Still, the simulated tNO_3 concentration ($\gamma_m(tNO_3)$) with GEOS-Chem is notably

272 overestimated relative to observations (γ_o(tNO$_3$); $B = 182$ %; **Figure 3**). While the simulated pNO$_3$

273 well reproduce the observed seasonality (high concentrations in the cold season and vice versa), it

274 highly overestimated the concentrations for most of the year ($B = 276$ %; **Figure 3**). The simulated

275 HNO$_3$ did not capture the observed relative lack of seasonality, instead showing clear seasonality

276 with generally high concentrations in the warm season and low in the cold season. The lack of

277 agreement between GEOS-Chem and nitrate observations is consistent with previously reported

278 results in other studies (Heald et al., 2012; Zhang et al., 2012; Walker et al., 2012). Uncertainties

279 in N$_2$O$_5$ hydrolysis rate, emission estimates, or dry and wet deposition removal rates have been

280 suggested as possible causes for predicted nitrate biases. For instance, Luo et al., 2019; 2020

281 reported dramatic improvement of nitric acid and nitrate biases by updating wet scavenging

282 parameterization in the GEOS-Chem model; however, this update leads to biases in oxidized

283 nitrogen wet deposition between model predictions and observations.

284

285 **3.2 Oxygen Isotopic Compositions – Oxidation Chemistry and Phase Difference**

286

287 The oxygen isotopic compositions in atmospheric nitrate are used to evaluate NO$_x$ oxidation

288 chemistry and to assess seasonal changes in nitrate formation mechanisms. For the CASTNET

289 sites, the Δ(^{17}O, HNO$_3$) and Δ(^{17}O, pNO$_3$) values ranged from 12.9 ‰ to 30.9 ‰ and from 16.6 ‰

290 to 33.7 ‰, with a mean value of (22.7±3.6) ‰ and (27.1±3.8) ‰, respectively **(Figure 4)**. The

291 δ(^{18}O, HNO$_3$) and δ(^{18}O, pNO$_3$) values ranged from 46.9 ‰ to 82.1 ‰ and from 43.6 ‰ to 85.3

292 ‰, with a mean value of (68.1±7.1) ‰ and (68.2±8.3) ‰, respectively **(Figure 5)**. These

293 observations are in the range of previously reported values in polluted mid-latitudes: δ(^{18}O, HNO$_3$)

294 and δ(^{18}O, pNO$_3$) in CASTNET sites in Ohio, Pennsylvania, and New York from April 2004 to

295 March 2005 ranged from 51.6 ‰ to 94.0 ‰ and from 45.2 ‰ to 92.7 ‰ (Elliott et al., 2009),

296 respectively. They are also consistent with observations of polluted air masses in Canada from

297 September 2010 to January 2014, which were from 62.4 to 81.7 ‰ for δ(^{18}O, HNO$_3$), from 19.3

298 to 29.0 ‰ for Δ(^{17}O, HNO$_3$), from 48.4 to 83.2 ‰ for δ(^{18}O, pNO$_3$), and from 13.8 to 30.5 ‰ for

299 Δ(^{17}O, pNO$_3$) (Savard et al., 2018).

300

301 Previous studies and modeling results have indicated that the seasonality of oxygen isotopic

302 compositions in HNO$_3$ and pNO$_3$ is driven by a shift in oxidation chemistry (e.g., Hastings et al.,

303   2003; Michalski et al, 2012; Alexander et al., 2009; 2020). Globally, the seasonality reflects a shift

304   in O_3 to HO_x radical chemistry during winter to summer, respectively. Wintertime has higher NO

305   + O_3 branching ratios than summer, which has increased NO + RO_2/HO_2. The high values of $\delta(^{18}O)$

306   and $\Delta(^{17}O)$ in HNO_3 and pNO_3 during the cold season are caused by the increased incorporation

307   of O_3 into the nitrate product through N_2O_5 heterogeneous hydrolysis on aerosols **(Figures 4 and**

308   **5)**. In contrast, the dominance of gas-phase production by the NO_2 + OH reaction dilutes the

309   isotopic influence of O_3 during warm seasons leading to the low values of $\delta(^{18}O)$ and $\Delta(^{17}O)$ in

310   HNO_3 and pNO_3. Spatial variability is observed in $\delta(^{18}O)$ and $\Delta(^{17}O)$ of HNO_3, with highest values

311   at CTH110 ($\delta(^{18}O)$: (71.5±5.6) ‰ (n = 24) and $\Delta(^{17}O)$: (25.0±3.1) ‰ (n = 23)) followed by

312   ABT147 ($\delta(^{18}O)$: (70.1±4.8) ‰ (n = 24) and $\Delta(^{17}O)$: (23.1±2.2) ‰ (n = 24)) and WST109 ($\delta(^{18}O)$:

313   (62.8±7.7) ‰ (n = 24) and $\Delta(^{17}O)$: (20.2±3.7) ‰ (n = 24)). However, $\delta(^{18}O)$ and $\Delta(^{17}O)$ of pNO_3

314   were not significantly different across the stations: for ABT147 ($\delta(^{18}O)$: (68.6±7.1) ‰ (n = 24)

315   and $\Delta(^{17}O)$: (26.4±3.6) ‰ (n = 22)); CTH110 ($\delta(^{18}O)$: (69.1±8.9) ‰ (n = 24) and $\Delta(^{17}O)$: (26.8±4.1)

316   ‰ (n = 19)); and WST109 ($\delta(^{18}O)$: (66.8±8.7) ‰ (n = 24) and $\Delta(^{17}O)$: (29.4±2.9) ‰ (n = 10)).

317

318   Our observations indicate a significant phase-dependent difference in oxidation chemistry between

319   HNO_3 and pNO_3 that is unexpected **(Figure 6)**. Many modeled mechanisms of gas- and aqueous-

320   phase chemistry produce HNO_3, then HNO_3 is partitioned into the aerosol phase based on

321   thermodynamic equilibrium (i.e., $NH_4NO_3(s) \rightleftharpoons HNO_3(g) + NH_3(g)$) or coarse uptake.

322   Conventional understanding would expect $\Delta(^{17}O)$ of HNO_3 and pNO_3 to be the same (e.g.,

323   Alexander., 2020). However, observed $\Delta(^{17}O, pNO_3)$ tends to be significantly higher than $\Delta(^{17}O,$

324    $HNO_3)$ ($p < 0.01$ at ABT and CTH, $p = 0.088$ at WST). The difference between $\Delta(^{17}O, pNO_3)$ and

325    $\Delta(^{17}O, HNO_3)$ was larger in the cold season than in the warm season. For example, on average,

326    $\Delta(^{17}O, pNO_3)$ was (5.1±2.6 ‰) higher than $\Delta(^{17}O, HNO_3)$ during the cold months, while $\Delta(^{17}O,$

327    $pNO_3)$ was (2.7±4.7 ‰) higher than $\Delta(^{17}O, HNO_3)$ during warm months. This phase difference in

328    $\Delta(^{17}O)$ cannot be explained by potential sample biases caused by volatilization, which leads to

329   mass-dependent fractionation. This difference might be related to the differences in particulate

330   nitrate size-dependent production pathways. Previous studies of size-segregated $\Delta(^{17}O, pNO_3)$

331   indicated higher values for coarse pNO_3 (aerodynamic diameter (D_a) > 0.95 μm) relative to fine

332   pNO_3 (D_a < 0.95 μm) that was concluded to reflect the increased importance of heterogeneous

333   N_2O_5 hydrolysis on coarse particles relative to fine particles (Vicars et al., 2013). The CASTNET

334 pNO$_3$ samples reflect total suspended particles (TSP) such that increased importance of N$_2$O$_5$

335 heterogeneous chemistry for coarse particulate nitrate formation could explain the higher $\Delta(^{17}$O,

336 pNO$_3$) values we observe relative to $\Delta(^{17}$O, HNO$_3$).

337

338 Positive linear relationships between $\delta(^{18}$O) and $\Delta(^{17}$O) were observed for HNO$_3$ and pNO$_3$ across

339 the CASTNET sites, with similar slopes but different oxygen isotopic signatures indicated by

340 different intercepts (**Figure 6**). For the relationship of $\delta(^{18}$O) and $\Delta(^{17}$O), the high end-member

341 should result from O$_3$, and the lower end-member depends on the isotopic signature of the

342 atmospheric oxidants involved. The transferable $\delta(^{18}$O) signatures of atmospheric oxidants are not

343 fully understood yet, reflecting a complex combination of atmospheric oxidant source signatures

344 and isotope fractionation during reaction and incorporation into the nitrate end-product. While

345 ozone has a notably high $\Delta(^{17}$O) value ((39±2) ‰; Vicars and Savarino, 2014), $\Delta(^{17}$O) values of

346 other atmospheric oxidants such as O$_2$/RO$_2$/HO$_2$, H$_2$O and OH are equal to or close to 0 ‰

347 (Michalski et al., 2012; Walters et al., 2019). Overall, our results suggest more O$_3$ is incorporated

348 during the formation of pNO$_3$ than HNO$_3$. We further analyze the oxidation chemistry involved in

349 atmospheric nitrate formation based on output from the GEOS-Chem chemical transport model.

350

351 **3.3 Quantifying atmospheric nitrate oxidation chemistry using $\Delta(^{17}$O)**

352 Observations of the oxygen isotopic composition were utilized to quantify the relative importance

353 of different nitrate formation pathways and to assess model representation of the chemistry of

354 nitrate formation. Using atmospheric nitrate production rates from the GEOS-Chem model ("base

355 case"), $\Delta(^{17}$O) was calculated within a grid cell corresponding to our CASTNET sites and

356 compared with observed $\Delta(^{17}$O, HNO$_3$, pNO$_3$) at each site **(Figure 4)**. We note that the previous

357 $\Delta(^{17}$O) GEOS-Chem framework tags NO$_2$ and HNO$_3$ production and assumes that pNO$_3$

358 production is similar to HNO$_3$ due to thermodynamic equilibrium. Thus, we compared the

359 simulated $\Delta(^{17}$O, HNO$_3$) from GEOS-Chem to our $\Delta(^{17}$O, HNO$_3$) and $\Delta(^{17}$O, pNO$_3$) observations.

360 The averaged residuals over the collection period for each site were 3.9 ‰, 2.8 ‰, and 5.6 ‰ for

361 $\Delta(^{17}$O, HNO$_3$), and 1.5 ‰, 1.7 ‰, and 6.1 ‰ for $\Delta(^{17}$O, pNO$_3$) at ABT147, CTH110, and WST109,

362 respectively **(Figure 4)**. Calculated $\Delta(^{17}$O) based on GEOS-Chem output reproduced the observed

363 temporal variations well **(Figure 4)**, although the model better captured the lower observed $\Delta(^{17}$O)

364 during warmer months versus the higher values observed in the cooler months (**Table 2**). The

365   GEOS-Chem model also does not capture observed spatial $\Delta(^{17}O)$ variabilities. For instance,

366   higher $\Delta(^{17}O)$ values (especially for HNO$_3$) were observed at CTH110 compared to WST109;

367   while no significant spatial $\Delta(^{17}O)$ differences were predicted from GEOS-Chem. The model

368   prediction was sensitive to the type of nitrate; the calculated $\Delta(^{17}O)$ showed a better agreement

369   with observed $\Delta(^{17}O)$ of pNO$_3$ ($y = 0.55\,x + 12.62$ ($R^2 = 0.48$)) than $\Delta(^{17}O)$ of HNO$_3$ ($y = 0.46\,x +$

370   10.68 ($R^2 = 0.44$)) at all CASTNET sites ($B = $ -2 % and 15 %, respectively) (**Figure 7**).

371

372   Several studies have used $\Delta(^{17}O)$ to quantify and/or constrain modeled chemical mechanisms. Here,

373   GEOS-Chem nitrate production rates and thus calculated $\Delta(^{17}O)$ were optimized to find the lowest

374   residual sum of squares between the calculated and observed $\Delta(^{17}O)$. This optimization algorithm

375   constrains the relative rates of nitrate formation pathways simulated by GEOS-Chem.

376   Additionally, the optimization was conducted for HNO$_3$ and pNO$_3$ separately. Calculated $\Delta(^{17}O)$

377   from the base GEOS-Chem model was generally 1.15 times higher than observed $\Delta(^{17}O,\ HNO_3)$

378   and 0.98 times lower than $\Delta(^{17}O,\ pNO_3)$ across all CASTNET sites. After optimization, the

379   residuals between observed and calculated $\Delta(^{17}O)$ dramatically decreased (**Figure 4),** especially in

380   the cold season **(Table 2**). Moreover, the linear relationships had slopes much closer to the 1:1 line

381   (i.e., from 0.46 to 1.03 for HNO$_3$ and from 0.55 to 0.78 for pNO$_3$**; Figure 7**) than the base GEOS-

382   Chem model across the three CASTNET site (the relationships for each site before and after

383   optimization are shown in **Figure 7**). On a subannnual basis, the $\Delta(^{17}O)$ comparison for the cold

384   season showed better improvement than the warm season, especially for $\Delta(^{17}O,\ HNO_3)$.

385

386   The dominant annual pathway for nitrate formation in the GEOS-Chem model ("base case") was

387   N$_2$O$_5$ hydrolysis, which accounts for 50 % **(Figure 8)**, followed by NO$_2$ + OH (31 %) and RONO$_2$

388   hydrolysis (13 %) across all CASTNET sites. Nitrate production via the reaction of XNO$_3$

389   hydrolysis and NO$_3$ + HC was small (< 1 %) at all sites. Strong seasonality in nitrate production

390   was observed, as expected, with high portions of N$_2$O$_5$ hydrolysis in winter and NO$_2$ + OH in

391   summer **(Figure 8)**.

392

393   After optimization, the dominant pathway for nitrate formation in GEOS-Chem changed compared

394   to the base case. For $\Delta(^{17}O,\ pNO_3)$, NO$_2$ + OH (60 %) was the dominant pathway for nitrate

395   formation in the optimized GEOS-Chem calculation, followed by N$_2$O$_5$ hydrolysis (31 %) and

396   NO$_3$ hydrolysis (4 %) **(Figure 8)**. At the same time, $\Delta(^{17}O, HNO_3)$ was almost entirely driven by

397   NO$_2$ + OH reaction (98 %) in the optimized GEOS-Chem case **(Figure 8)**. The optimized GEOS-

398   Chem calculations suggest that the fraction of nitrate produced by N$_2$O$_5$ hydrolysis was

399   significantly overestimated in the GEOS-Chem base case. In the base case, N$_2$O$_5$ hydrolysis

400   dominated nitrate production, especially in the cold season with a fraction of over 68 % at all

401   CASTNET sites **(Figure 8)**. This may also partly explain major nitrate concentration overestimates,

402   particularly in the cold season.

403

404   **3.4 Modeling $\delta(^{18}O)$ of Atmospheric Nitrate**

405   The GEOS-Chem model $\delta(^{18}O)$ was also calculated in the same manner as $\Delta(^{17}O)$ **(Figure 5)**.

406   Unlike the calculated $\Delta(^{17}O)$, calculated $\delta(^{18}O)$ showed remarkably positive biases compared with

407   measured $\delta(^{18}O)$ of HNO$_3$ (B = 22 %) and pNO$_3$ (B = 21 %). The averaged residuals for $\delta(^{18}O,$

408   HNO$_3$) at each site were 13.9 ‰, 12.9 ‰, and 19.6 ‰, and for $\delta(^{18}O, pNO_3)$ were 15.4 ‰, 14.2

409   ‰, and 18.2 ‰ at ABT147, CTH110, and WST109, respectively **(Figure 5, Table 2)**. Modeling

410   the $\delta(^{18}O)$ values of nitrate is more challenging than $\Delta(^{17}O)$ because not all oxidant $\delta(^{18}O)$ values

411   have been directly observed and fractionation factors associated with the O transfer into NO$_y$

412   products are unknown. Uncertainty in $\delta(^{18}O)$ values could be a major factor causing disagreement

413   between observed and calculated $\delta(^{18}O)$. Additionally, uncertainties in the gas-phase and aerosol

414   scheme related to tNO$_3$ production in GEOS-Chem could account for the discrepancy. Still, as

415   with $\Delta(^{17}O)$, the calculated $\delta(^{18}O)$ showed far more disagreement with observations during cooler

416   months than warmer months **(Table 2)**.

417

418   Newly optimized nitrate production in GEOS-Chem was also applied to $\delta(^{18}O)$ calculation and

419   compared with previous results. As with $\Delta(^{17}O)$, a slope of the regression line between (optimized)

420   calculated and observed $\delta(^{18}O)$ became closer to 1 (i.e., from 0.30 to 0.74 for HNO$_3$ and from 0.39

421   to 0.49 for pNO$_3$; **Figure 9**) and residuals improved at each site after the optimization **(Figure 5)**.

422   Overall, the optimized GEOS-Chem $\delta(^{18}O)$ calculation showed better agreement than the base

423   GEOS-Chem model (B = -6 % for $\delta(^{18}O, HNO_3)$ and B = 13 % for $\delta(^{18}O, pNO_3)$). The most

424   significant improvement, as shown by the residuals, is during the cold season.

425

426   **3.5 $\delta(^{18}O)$ Optimization of Atmospheric Oxidants**

427 After optimization of relative nitrate production rates in GEOS-Chem based on $\Delta(^{17}O)$, we applied

428 the optimized chemical production to calculate $\delta(^{18}O)$, but still observed discrepancy between

429 observed and predicted $\delta(^{18}O)$. The discrepancy could be related to variable and somewhat

430 unconstrained $\delta(^{18}O)$ values of atmospheric oxidants important for nitrate formation. To test this,

431 the assumed (literature) $\delta(^{18}O)$ values of oxidants were optimized by selecting the best linear fit

432 between the observations and calculated $\delta(^{18}O, HNO_3$ and $pNO_3)$ **(Figure 10)**. After optimization

433 for $\delta(^{18}O)$ of oxidants, the discrepancy between observation and calculation was dramatically

434 reduced **(Figure 9)** with a decrease in B from 21 to 1 %. The optimization predicted $\delta(^{18}O)$ of H_2O

435 values similar to what was expected (-6.5 ‰ vs. -6.0 ‰), however different values were predicted

436 for $\delta(^{18}O)$ of O_2, OH, and O_3 (**Table 3**). A typical mid-latitude value (-6 ‰) of $\delta(^{18}O, H_2O)$ was

437 selected in this study. We note that the $\delta(^{18}O, H_2O)$ will vary seasonally; however, the calculated

438 $\delta(^{18}O)$ value of nitrate was insensitive to this value because of the relatively minor role that H_2O

439 contributes to O atoms of atmospheric nitrate. For $\delta(^{18}O)$ of O_2, OH, and O_3, it is possible that this

440 reflects isotope effects associated with the incorporation of these oxidants during nitrate

441 production, rather than further issues with model chemistry since the relative production rates here

442 are constrained based on $\Delta(^{17}O)$. The $\delta(^{18}O, O_2)$ was the best fit with calculated $\delta(^{18}O)$ of nitrate

443 values when assuming a value of 11.1 ‰ (vs. the well-known 23 ‰). Since atmospheric O_2 is

444 incorporated into nitrate via NO oxidation by HO_2 and RO_2 radicals, it was assumed that the $\delta(^{18}O)$

445 value of RO_2 and HO_2 is equal to O_2 such that this does not consider any potential isotope effects

446 associated with HO_2 and RO_2 formation and reaction with NO. The optimized value of 11 ‰

447 reflects the O atom derived from RO_2/HO_2 reactions incorporated into NO_2. Thus, our optimized

448 value might suggest that RO_2/HO_2 singly substituted with ^{18}O (e.g., $R^{18}O^{16}O$, $H^{18}O^{16}O$) reacts

449 slower than the ^{16}O isotopologues (e.g., $R^{16}O_2$ or $H^{16}O_2$).

450

451 The observed $\delta(^{18}O)$ of O_3 and OH for the CASTNET samples were the best fit with calculated

452 $\delta(^{18}O)$ when assuming values of 89.9 ‰ for $\delta(^{18}O, O_3)$ and 42.2 ‰ for $\delta(^{18}O, OH)$, respectively.

453 In the previous section, we noted that NO_2 + OH and N_2O_5 hydrolysis reactions were the dominant

454 pathways for nitrate formation, indicating that OH and O_3 play an important role in determining

455 the $\delta(^{18}O)$ value in nitrate. Indeed, optimizing $\delta(^{18}O)$ values to find the best agreement between

456 observation and calculation is largely dependent on $\delta(^{18}O)$ values of O_3 and OH (see also **Table**

457 **3**). The optimized $\delta(^{18}O, O_3{}^*)$ value (89.9 ‰) was lower than the average reported $\delta(^{18}O, O_3{}^*)$

458 ((~126±12) ‰; Vicars and Savarino, 2014), though the $\delta(^{18}O, O_3)$ is known to vary with
459 temperature and pressure, and could also potentially be fractionated during reactions
460 (Brenninkmeijer et al., 2004). For example, Walters and Michalski (2016) calculated an isotopic
461 enrichment factor near -20 ‰ associated with O_3 transfer in its reaction with NO, which would
462 lower the transferable $\delta(^{18}O)$ of O_3, consistent with our predictions. The isotope effect for NO +
463 O_3 reaction is the only one currently known; in other words, no other $\delta(^{18}O)$ isotope effects
464 associated with O_3 reaction with NO_y (e.g., $NO_2 + O_3$) have been calculated. Further, there is
465 potential for equilibrium isotope effects between N_2O_5, NO_2, and NO_3 that could also impart a
466 mass-dependent $\delta(^{18}O)$ fractionation. While difficult to pinpoint the exact isotope effects occurring,
467 our optimized value predicts an elevated $\delta(^{18}O)$ value derived from O_3 compared to the other
468 oxidants, consistent with our expectation.

469

470 For $\delta(^{18}O, OH)$, the optimized value dramatically increased compared to the initial assumed value
471 (-43.0 ‰). The initial $\delta(^{18}O, OH)$ value is based on several assumptions that may not be correct
472 regarding isotope exchange with $H_2O(g)$. Additionally, Fang et al. (2021) suggested that $\delta(^{15}N)$ of
473 nitrate is largely controlled by an isotope effect in the $NO_2 + OH$ pathway, and it could be
474 conceivable that $\delta(^{18}O)$ may be affected by a similar isotope effect as well. Overall, the
475 optimization of $\delta(^{18}O, OH)$ is highly dependent on the $\delta(^{18}O, O_3^*)$ (see **Table 3),** which makes
476 sense given the proportional control of the $NO_2 + OH$ and N_2O_5 hydrolysis reactions. Despite the
477 uncertainty in the transferrable $\delta(^{18}O)$ from major oxidants, the comparison between predicted and
478 observed $\delta(^{18}O)$ and $\Delta(^{17}O)$ both suggest a larger relative importance of $NO_2 +OH$ chemistry than
479 reflected in the model simulations. We note here that this finding is consistent with our companion
480 study (acp-2022-621) of $\delta(^{15}N, HNO_3)$ and $\delta(^{15}N, pNO_3)$ as well.

481

482 Overall, the observed differences in the oxygen isotopic composition of HNO_3 and pNO_3, the
483 observed relationships of $\delta(^{18}O)$ and $\Delta(^{17}O)$ in the different nitrate phases, and the significant
484 mismatch with the global model base case challenge our current representation of nitrate chemistry
485 in atmospheric chemistry models. Generally, the GEOS-Chem $\Delta(^{17}O)$ simulations were biased
486 high relative to observations, indicating the over-incorporation of O_3 during nitrate formation. The
487 largest discrepancies in the model-observation comparisons, particularly for pNO_3, occur in winter.
488 Our optimized chemistry, constrained by the observed $\delta(^{18}O)$ and $\Delta(^{17}O)$, suggested that the

489   heterogenous production of nitrate via N_2O_5 chemistry is currently significantly overestimated.
490   While our focus is on the northeastern US, an area of important environmental change due to
491   regulated emissions reductions, this finding has implications for the global modeling of
492   atmospheric nitrate and oxidation chemistry.

493

494   **4. Conclusions**

495

496   Using a combination of concentration and isotopic analyses, we evaluated atmospheric nitrate
497   formation pathways in the northeastern US in 2017–2018. The GEOS-Chem model showed large
498   positive biases for HNO_3 and pNO_3 concentrations, an important issue that is common in
499   atmospheric chemistry models. The observed oxygen isotopic compositions ($\Delta(^{17}O)$ and $\delta(^{18}O)$)
500   revealed a more important relative role of NO_2+OH chemistry and indicated that the model
501   chemistry overpredicted heterogeneous hydrolysis of N_2O_5 for atmospheric nitrate in the
502   northeastern US. We also observed nitrate-phase differences in $\Delta(^{17}O)$ and $\delta(^{18}O)$, which are not
503   captured in current models. Further investigation of size-segregated nitrate chemistry is
504   recommended to improve model prediction of nitrate formation.

505

506   Additionally, this finding has important implications for predicting oxidation chemistry in the
507   atmosphere. For instance, the production of nitrate via heterogeneous hydrolysis of N_2O_5
508   represents a radical termination process, such that a much-reduced importance of this reaction
509   could yield more radical chemistry with an impact on oxidant concentrations. Indeed, an important
510   mechanism for converting NO_x to atmospheric nitrate could affect controlling the oxidizing
511   efficiency, which directly influences the atmospheric oxidation budget and many atmospheric
512   pollutants' (notably greenhouse gases) lifetime in the atmosphere. Thus, better constraining their
513   chemistries and feedbacks is crucial to understanding atmospheric nitrate production pathways and
514   its connection to atmospheric oxidation chemistry.

515

516   Traditionally, $\Delta(^{17}O)$ has been used to quantitatively assess nitrate production pathways. The use
517   of $\delta(^{18}O)$ as well can enhance our understanding of the oxidants contributing to nitrate formation,
518   particularly for distinguishing oxidants that have similar $\Delta(^{17}O)$ values (i.e., all are near 0 ‰ except
519   ozone). However, our study also observed a discrepancy between observed and calculated $\delta(^{18}O)$

520 values, even after accounting for an optimized chemical production based on $\Delta(^{17}O)$. The best
521 match of the observations suggests that the transferrable $\delta(^{18}O)$ values of oxidants may vary more
522 than is currently suggested in the literature. Improved constraints, particularly on the isotopic
523 composition of OH and variability in $\delta(^{18}O, O_3)$ would add critical value to modeling and
524 interpretation of major oxidation chemistry in the atmosphere.

525

526 **Data Availability.** Data presented in this article are available on the Harvard Dataverse at
527 https://doi.org/10.7910/DVN/X6BB1I, US EPA CASTNET database.

528

529 **Author Contributions.** HK, WWW, MGH designed the varying aspects of the study. CB and
530 WWW carried out the laboratory measurements. HK interpreted data, conducted statistical
531 analysis, and analyzed model results. LTM contributed GEOS-Chem simulations. HK and WWW
532 prepared the article with contributions from all co-authors.

533

534 **Acknowledgements.** We thank Ruby Ho for sampling and laboratory assistance. We are grateful
535 to the US EPA CASTNET program and staff for their cooperation in this study and assistance with
536 receiving archived samples for isotopic analysis.

537

538 **Competing Interests.** The authors declare no competing financial interest.

539

540 **Financial Support.**   National Science Foundation (AGS-2002750); Institute at Brown for
541 Environment and Society Seed Grant; Voss Environmental Fellowship from the Institute at Brown
542 for Environment and Society

543
544
545 **Reference**

546
547 Alexander, B., Hastings, M. G., Allman, D. J., Dachs, J., Thornton, J. A., and Kunasek, S. A.:
548   Quantifying atmospheric nitrate formation pathways based on a global model of the oxygen
549   isotopic composition ($\Delta^{17}O$) of atmospheric nitrate, Atmospheric Chemistry and Physics, 9,
550   5043–5056, 2009.
551 Alexander, B., Sherwen, T., Holmes, C. D., Fisher, J. A., Chen, Q., Evans, M. J., and Kasibhatla,
552   P.: Global inorganic nitrate production mechanisms: comparison of a global model with nitrate
553   isotope observations, Atmospheric Chemistry and Physics, 20, 3859–3877, 2020.

Amos, H. M., Jacob, D. J., Holmes, C. D., Fisher, J. A., Wang, Q., Yantosca, R. M., Corbitt, E. S., Galarneau, E., Rutter, A. P., and Gustin, M. S.: Gas-particle partitioning of atmospheric Hg (II) and its effect on global mercury deposition, Atmospheric Chemistry and Physics, 12, 591–603, 2012.

Ashbaugh, L. L. and Eldred, R. A.: Loss of Particle Nitrate from Teflon Sampling Filters: Effects on Measured Gravimetric Mass in California and in the IMPROVE Network, Journal of the Air & Waste Management Association, 54, 93–104, https://doi.org/10.1080/10473289.2004.10470878, 2004.

Bates, K. H. and Jacob, D. J.: A new model mechanism for atmospheric oxidation of isoprene: global effects on oxidants, nitrogen oxides, organic products, and secondary organic aerosol, Atmospheric Chemistry and Physics, 19, 9613–9640, 2019.

Bekker, C., Walters, W.W., L. T. Murray, and Hastings, M. G.: Nitrate Chemistry in the Northeast US-Part I: Nitrogen Isotopic Seasonality Tracks with Nitrate Formation Chemistry, Atmospheric Chemistry and Physics Discussions, 2023.

Bey, I., Jacob, D. J., Yantosca, R. M., Logan, J. A., Field, B. D., Fiore, A. M., Li, Q., Liu, H. Y., Mickley, L. J., and Schultz, M. G.: Global modeling of tropospheric chemistry with assimilated meteorology: Model description and evaluation, Journal of Geophysical Research: Atmospheres, 106, 23073–23095, 2001.

Breider, T. J., Mickley, L. J., Jacob, D. J., Ge, C., Wang, J., Payer Sulprizio, M., Croft, B., Ridley, D. A., McConnell, J. R., and Sharma, S.: Multidecadal trends in aerosol radiative forcing over the Arctic: Contribution of changes in anthropogenic aerosol to Arctic warming since 1980, Journal of Geophysical Research: Atmospheres, 122, 3573–3594, 2017.

Brenninkmeijer, C. A., Janssen, C., Kaiser, J., Röckmann, T., Rhee, T. S., and Assonov, S. S.: Isotope effects in the chemistry of atmospheric trace compounds, Chemical Reviews, 103, 5125–5162, 2003.

Camargo, J. A. and Alonso, Á.: Ecological and toxicological effects of inorganic nitrogen pollution in aquatic ecosystems: a global assessment, Environment international, 32, 831–849, 2006.

Carter, T. (Tess) S., Joyce, E. E., and Hastings, M. G.: Quantifying Nitrate Formation Pathways in the Equatorial Pacific Atmosphere from the GEOTRACES Peru-Tahiti Transect, ACS Earth and Space Chemistry, 5, 2638–2651, 2021.

Casciotti, K. L., Sigman, D. M., Hastings, M. G., Böhlke, J. K., and Hilkert, A.: Measurement of the oxygen isotopic composition of nitrate in seawater and freshwater using the denitrifier method, Analytical chemistry, 74, 4905–4912, 2002.

CASTNET (Clean Air Status and Trends Network), Retrieved from United States Environmental Protection Agency, available at https://www.epa.gov/castnet, 2019

Crutzen, P. J.: The role of NO and NO_2 in the chemistry of the troposphere and stratosphere, Annual review of earth and planetary sciences, 7, 443–472, 1979.

Dubey, M. K., Mohrschladt, R., Donahue, N. M., and Anderson, J. G.: Isotope specific kinetics of hydroxyl radical (OH) with water (H_2O): Testing models of reactivity and atmospheric fractionation, The Journal of Physical Chemistry A, 101, 1494–1500, 1997.

Elliott, E. M., Kendall, C., Boyer, E. W., Burns, D. A., Lear, G. G., Golden, H. E., Harlin, K., Bytnerowicz, A., Butler, T. J., and Glatz, R.: Dual nitrate isotopes in dry deposition: Utility for partitioning NO_x source contributions to landscape nitrogen deposition, Journal of Geophysical Research: Biogeosciences, 114, 2009.

Fang, H., Walters, W. W., Mase, D., and Michalski, G.: i_NRACM: incorporating ^{15}N into the Regional Atmospheric Chemistry Mechanism (RACM) for assessing the role photochemistry plays in controlling the isotopic composition of NO_x, NO_y, and atmospheric nitrate, Geoscientific Model Development, 14, 5001–5022, 2021.

Fountoukis, C. and Nenes, A.: ISORROPIA II: a computationally efficient thermodynamic equilibrium model for $K^+–Ca^{2+}–Mg^{2+}–NH^{4+}–Na^+–SO_4^{2-}–NO_3^-–Cl^-–H_2O$ aerosols, Atmospheric Chemistry and Physics, 7, 4639–4659, 2007.

Galloway, J. N., Dentener, F. J., Capone, D. G., Boyer, E. W., Howarth, R. W., Seitzinger, S. P., Asner, G. P., Cleveland, C. C., Green, P. A., and Holland, E. A.: Nitrogen cycles: past, present, and future, Biogeochemistry, 70, 153–226, 2004.

Guenther, A. B., Jiang, X., Heald, C. L., Sakulyanontvittaya, T., Duhl, T. any, Emmons, L. K., and Wang, X.: The Model of Emissions of Gases and Aerosols from Nature version 2.1 (MEGAN2. 1): an extended and updated framework for modeling biogenic emissions, Geoscientific Model Development, 5, 1471–1492, 2012.

Hastings, M. G., Sigman, D. M., and Lipschultz, F.: Isotopic evidence for source changes of nitrate in rain at Bermuda, Journal of Geophysical Research: Atmospheres, 108, 2003.

Heald, C. L., Collett Jr, J. L., Lee, T., Benedict, K. B., Schwandner, F. M., Li, Y., Clarisse, L., Hurtmans, D. R., Van Damme, M., and Clerbaux, C.: Atmospheric ammonia and particulate inorganic nitrogen over the United States, Atmospheric Chemistry and Physics, 12, 10295–10312, 2012.

Hering, S. and Cass, G.: The magnitude of bias in the measurement of $PM_{2.5}$ arising from volatilization of particulate nitrate from Teflon filters, Journal of the Air & Waste Management Association, 49, 725–733, 1999.

Hoesly, R. M., Smith, S. J., Feng, L., Klimont, Z., Janssens-Maenhout, G., Pitkanen, T., Seibert, J. J., Vu, L., Andres, R. J., and Bolt, R. M.: Historical (1750–2014) anthropogenic emissions of reactive gases and aerosols from the Community Emissions Data System (CEDS), Geoscientific Model Development, 11, 369–408, 2018.

Holt, J., Selin, N. E., and Solomon, S.: Changes in inorganic fine particulate matter sensitivities to precursors due to large-scale US emissions reductions, Environmental Science & Technology, 49, 4834–4841, 2015.

Hu, L., Millet, D. B., Baasandorj, M., Griffis, T. J., Turner, P., Helmig, D., Curtis, A. J., and Hueber, J.: Isoprene emissions and impacts over an ecological transition region in the US Upper Midwest inferred from tall tower measurements, Journal of Geophysical Research: Atmospheres, 120, 3553–3571, 2015.

Huang, J. and Jaeglé, L.: Wintertime enhancements of sea salt aerosol in polar regions consistent with a sea ice source from blowing snow, Atmospheric Chemistry and Physics, 17, 3699–3712, 2017.

635   Hudman, R. C., Moore, N. E., Martin, R. V., Russell, A. R., Mebust, A. K., Valin, L. C., and
636   Cohen, R. C.: A mechanistic model of global soil nitric oxide emissions: implementation and
637   space based-constraints., Atmospheric Chemistry & Physics Discussions, 12, 2012.

638   Jaeglé, L., Quinn, P. K., Bates, T. S., Alexander, B., and Lin, J.-T.: Global distribution of sea salt
639   aerosols: new constraints from in situ and remote sensing observations, Atmospheric
640   Chemistry and Physics, 11, 3137–3157, 2011.

641   Jaeglé, L., Shah, V., Thornton, J. A., Lopez-Hilfiker, F. D., Lee, B. H., McDuffie, E. E., Fibiger,
642   D., Brown, S. S., Veres, P., and Sparks, T. L.: Nitrogen oxides emissions, chemistry,
643   deposition, and export over the Northeast United States during the WINTER aircraft campaign,
644   Journal of Geophysical Research: Atmospheres, 123, 12–368, 2018.

645   Kaiser, J., Hastings, M. G., Houlton, B. Z., Röckmann, T., and Sigman, D. M.: Triple oxygen
646   isotope analysis of nitrate using the denitrifier method and thermal decomposition of N2O,
647   Analytical Chemistry, 79, 599–607, 2007.

648   Kasibhatla, P., Sherwen, T., Evans, M. J., Carpenter, L. J., Reed, C., Alexander, B., Chen, Q.,
649   Sulprizio, M. P., Lee, J. D., and Read, K. A.: Global impact of nitrate photolysis in sea-salt
650   aerosol on NO_x, OH, and O_3 in the marine boundary layer, Atmospheric Chemistry and Physics,
651   18, 11185–11203, 2018.

652   Kroopnick, P. and Craig, H.: Atmospheric oxygen: isotopic composition and solubility
653   fractionation, Science, 175, 54–55, 1972.

654   Liu, H., Jacob, D. J., Bey, I., and Yantosca, R. M.: Constraints from ^{210}Pb and ^{7}Be on wet
655   deposition and transport in a global three-dimensional chemical tracer model driven by
656   assimilated meteorological fields, Journal of Geophysical Research: Atmospheres, 106,
657   12109–12128, 2001.

658   Luo, G., Yu, F., and Moch, J. M.: Further improvement of wet process treatments in GEOS-Chem
659   v12.6.0: impact on global distributions of aerosols and aerosol precursors, Geoscientific Model
660   Development, 13, 2879–2903, 2020.

661   Luo, G., Yu, F., and Schwab, J.: Revised treatment of wet scavenging processes dramatically
662   improves GEOS-Chem 12.0.0 simulations of surface nitric acid, nitrate, and ammonium over
663   the United States, Geoscientific Model Development, 12, 3439–3447, 2019.

664   McDuffie, E. E., Smith, S. J., O'Rourke, P., Tibrewal, K., Venkataraman, C., Marais, E. A., Zheng,
665   B., Crippa, M., Brauer, M., and Martin, R. V.: A global anthropogenic emission inventory of
666   atmospheric pollutants from sector- and fuel-specific sources (1970–2017): an application of
667   the Community Emissions Data System (CEDS), Earth System Science Data, 12, 3413–3442,
668   https://doi.org/10.5194/essd-12-3413-2020, 2020.

669   Michalski, G., Bhattacharya, S. K., and Mase, D. F.: Oxygen isotope dynamics of atmospheric
670   nitrate and its precursor molecules, in: Handbook of environmental isotope geochemistry,
671   Springer, 613–635, 2012.

672   Michalski, G., Scott, Z., Kabiling, M., and Thiemens, M. H.: First measurements and modeling of
673   Δ^{17}O in atmospheric nitrate, Geophysical Research Letters, 30, 2003.

674   Millet, D. B., Guenther, A., Siegel, D. A., Nelson, N. B., Singh, H. B., de Gouw, J. A., Warneke,
675   C., Williams, J., Eerdekens, G., Sinha, V., Karl, T., Flocke, F., Apel, E., Riemer, D. D., Palmer,
676   P. I., and Barkley, M.: Global atmospheric budget of acetaldehyde: 3-D model analysis and
677   constraints from in-situ and satellite observations, Atmospheric Chemistry and Physics, 10,
678   3405–3425, https://doi.org/10.5194/acp-10-3405-2010, 2010.

679   Morin, S., Sander, R., and Savarino, J.: Simulation of the diurnal variations of the oxygen isotope
680   anomaly ($\Delta^{17}O$) of reactive atmospheric species, Atmospheric Chemistry and Physics, 11,
681   3653–3671, 2011.

682   Murray, L. T., Jacob, D. J., Logan, J. A., Hudman, R. C., and Koshak, W. J.: Optimized regional
683   and interannual variability of lightning in a global chemical transport model constrained by
684   LIS/OTD satellite data, Journal of Geophysical Research: Atmospheres, 117, 2012.

685   NEI (National Emissions Inventory): Retrieved from United States Environmental Protection
686   Agency, available at https://www.epa.gov/air-emissions-inventories/national-emissions-
687   inventory-nei, 2017.

688   Ridley, D. A., Heald, C. L., and Ford, B.: North African dust export and deposition: A satellite and
689   model perspective, Journal of Geophysical Research: Atmospheres, 117, 2012.

690   Savard, M. M., Cole, A. S., Vet, R., and Smirnoff, A.: The $\Delta^{17}O$ and $\delta^{18}O$ values of atmospheric
691   nitrates simultaneously collected downwind of anthropogenic sources–implications for
692   polluted air masses, Atmospheric Chemistry and Physics, 18, 10373–10389, 2018.

693   Savarino, J., Kaiser, J., Morin, S., Sigman, D. M., and Thiemens, M. H.: Nitrogen and oxygen
694   isotopic constraints on the origin of atmospheric nitrate in coastal Antarctica, Atmospheric
695   Chemistry and Physics, 7, 1925–1945, 2007.

696   Schlesinger, R. B.: The health impact of common inorganic components of fine particulate matter
697   (PM2. 5) in ambient air: a critical review, Inhalation toxicology, 19, 811–832, 2007.

698   Shah, V., Jaeglé, L., Thornton, J. A., Lopez-Hilfiker, F. D., Lee, B. H., Schroder, J. C.,
699   Campuzano-Jost, P., Jimenez, J. L., Guo, H., and Sullivan, A. P.: Chemical feedbacks weaken
700   the wintertime response of particulate sulfate and nitrate to emissions reductions over the
701   eastern United States, Proceedings of the National Academy of Sciences, 115, 8110–8115,
702   2018.

703   Sickles Ii, J. E. and Shadwick, D. S.: Air quality and atmospheric deposition in the eastern US: 20
704   years of change, Atmospheric Chemistry and Physics, 15, 173–197, 2015.

705   Sigman, D. M., Casciotti, K. L., Andreani, M., Barford, C., Galanter, M., and Böhlke, J. K.: A
706   bacterial method for the nitrogen isotopic analysis of nitrate in seawater and freshwater,
707   Analytical chemistry, 73, 4145–4153, 2001.

708   Tai, A. P., Mickley, L. J., and Jacob, D. J.: Correlations between fine particulate matter ($PM_{2.5}$)
709   and meteorological variables in the United States: Implications for the sensitivity of $PM_{2.5}$ to
710   climate change, Atmospheric environment, 44, 3976–3984, 2010.

711   Thiemens, M. H.: History and applications of mass-independent isotope effects, Annu. Rev. Earth
712   Planet. Sci., 34, 217–262, 2006.

US EPA (Environmental Protection Agency): Our nation's air, available at https://gispub.epa.gov/air/trendsreport/ 2017/, 2017.

van der Werf, G. R., Randerson, J. T., Giglio, L., van Leeuwen, T. T., Chen, Y., Rogers, B. M., Mu, M., van Marle, M. J. E., Morton, D. C., Collatz, G. J., Yokelson, R. J., and Kasibhatla, P. S.: Global fire emissions estimates during 1997–2016, Earth System Science Data, 9, 697–720, https://doi.org/10.5194/essd-9-697-2017, 2017.

Vicars, W. C. and Savarino, J.: Quantitative constraints on the ^{17}O-excess (Δ^{17}O) signature of surface ozone: Ambient measurements from 50°N to 50°S using the nitrite-coated filter technique, Geochimica et Cosmochimica Acta, 135, 270–287, 2014.

Vicars, W. C., Bhattacharya, S. K., Erbland, J., and Savarino, J.: Measurement of the ^{17}O-excess (Δ^{17}O) of tropospheric ozone using a nitrite-coated filter, Rapid Communications in Mass Spectrometry, 26, 1219–1231, 2012.

Vicars, W. C., Morin, S., Savarino, J., Wagner, N. L., Erbland, J., Vince, E., Martins, J. M. F., Lerner, B. M., Quinn, P. K., and Coffman, D. J.: Spatial and diurnal variability in reactive nitrogen oxide chemistry as reflected in the isotopic composition of atmospheric nitrate: Results from the CalNex 2010 field study, Journal of Geophysical Research: Atmospheres, 118, 10–567, 2013.

Walker, J. M., Philip, S., Martin, R. V., and Seinfeld, J. H.: Simulation of nitrate, sulfate, and ammonium aerosols over the United States, Atmospheric Chemistry and Physics, 12, 11213–11227, 2012.

Walker, J. T., Beachley, G., Amos, H. M., Baron, J. S., Bash, J., Baumgardner, R., Bell, M. D., Benedict, K. B., Chen, X., and Clow, D. W.: Toward the improvement of total nitrogen deposition budgets in the United States, Science of the Total Environment, 691, 1328–1352, 2019.

Walters, W. W. and Michalski, G.: Theoretical calculation of oxygen equilibrium isotope fractionation factors involving various NO_y molecules, OH, and H_2O and its implications for isotope variations in atmospheric nitrate, Geochimica et Cosmochimica Acta, 191, 89–101, 2016.

Walters, W. W., Fang, H., and Michalski, G.: Summertime diurnal variations in the isotopic composition of atmospheric nitrogen dioxide at a small midwestern United States city, Atmospheric Environment, 179, 1–11, 2018.

Walters, W. W., Michalski, G., Böhlke, J. K., Alexander, B., Savarino, J., and Thiemens, M. H.: Assessing the seasonal dynamics of nitrate and sulfate aerosols at the South Pole utilizing stable isotopes, Journal of Geophysical Research: Atmospheres, 124, 8161–8177, 2019.

Wang, X., Jacob, D. J., Downs, W., Zhai, S., Zhu, L., Shah, V., Holmes, C. D., Sherwen, T., Alexander, B., and Evans, M. J.: Global tropospheric halogen (Cl, Br, I) chemistry and its impact on oxidants, Atmospheric Chemistry and Physics, 21, 13973–13996, 2021.

Wesely, M. L. and Lesht, B. M.: Comparison of RADM dry deposition algorithms with a site-specific method for inferring dry deposition, Water, Air, and Soil Pollution, 44, 273–293, 1989.

752 Zhang, L., Jacob, D. J., Knipping, E. M., Kumar, N., Munger, J. W., Carouge, C. C., Van
753   Donkelaar, A., Wang, Y. X., and Chen, D.: Nitrogen deposition to the United States:
754   distribution, sources, and processes, Atmospheric Chemistry and Physics, 12, 4539–4554,
755   2012.

756
757
758
759
760
761
762
763
764
765
766
767
768
769
770
771
772
773
774
775
776
777
778
779
780
781
782
783
784
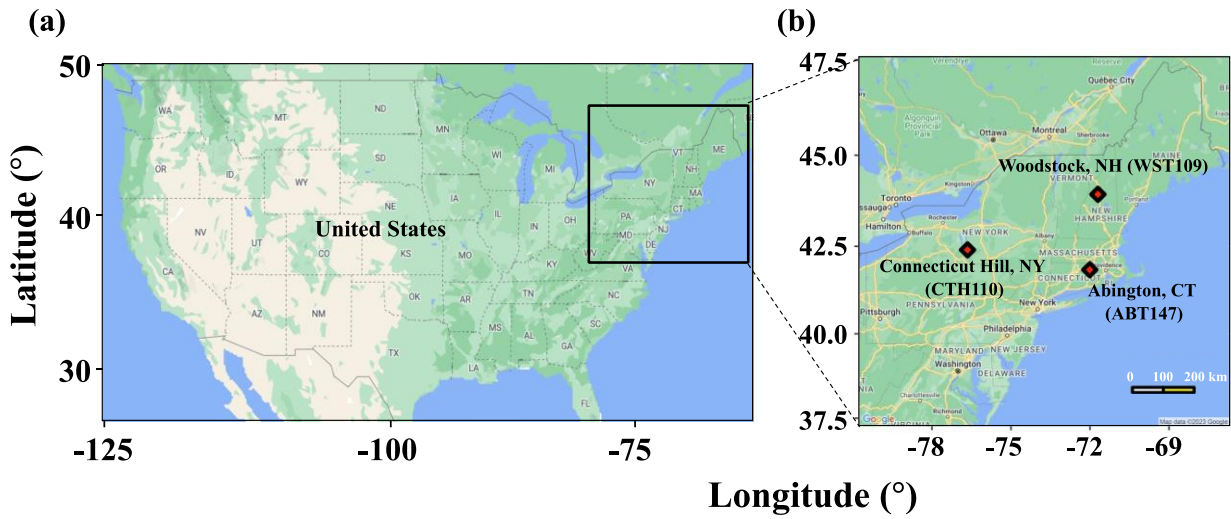
785
786 **Figure 1. Map of the United States (a) and selected CASTNET sites (b) for this study in the**
787 **northeastern US. Major cities (urban areas), transportation routes, and CASTNET sites are**
788 **also indicated in (b). The image was created using Google Earth (©2023 Google).**

789
790
791
792
793
794
795
796
797
798
799

(a) HNO₃
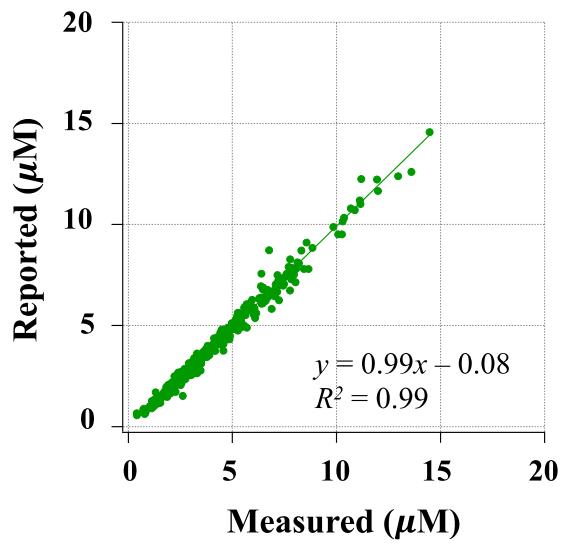
(b) pNO₃
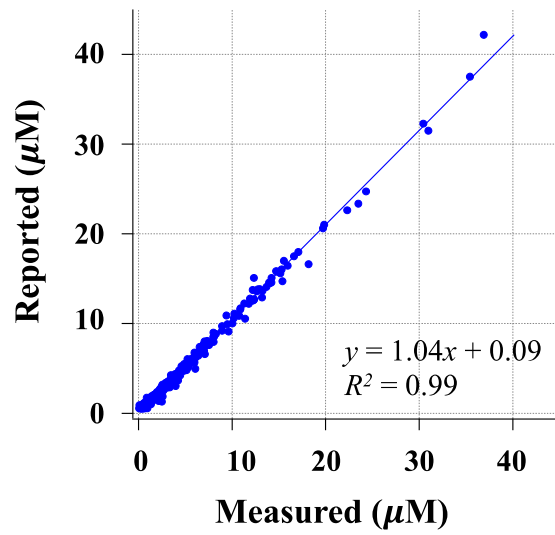
800

801 **Figure 2. Relationship of HNO₃ (a) and pNO₃ (b) filter extract concentrations reported by**

802 **CASTNET and re-measured at Brown University.**

803

804

805
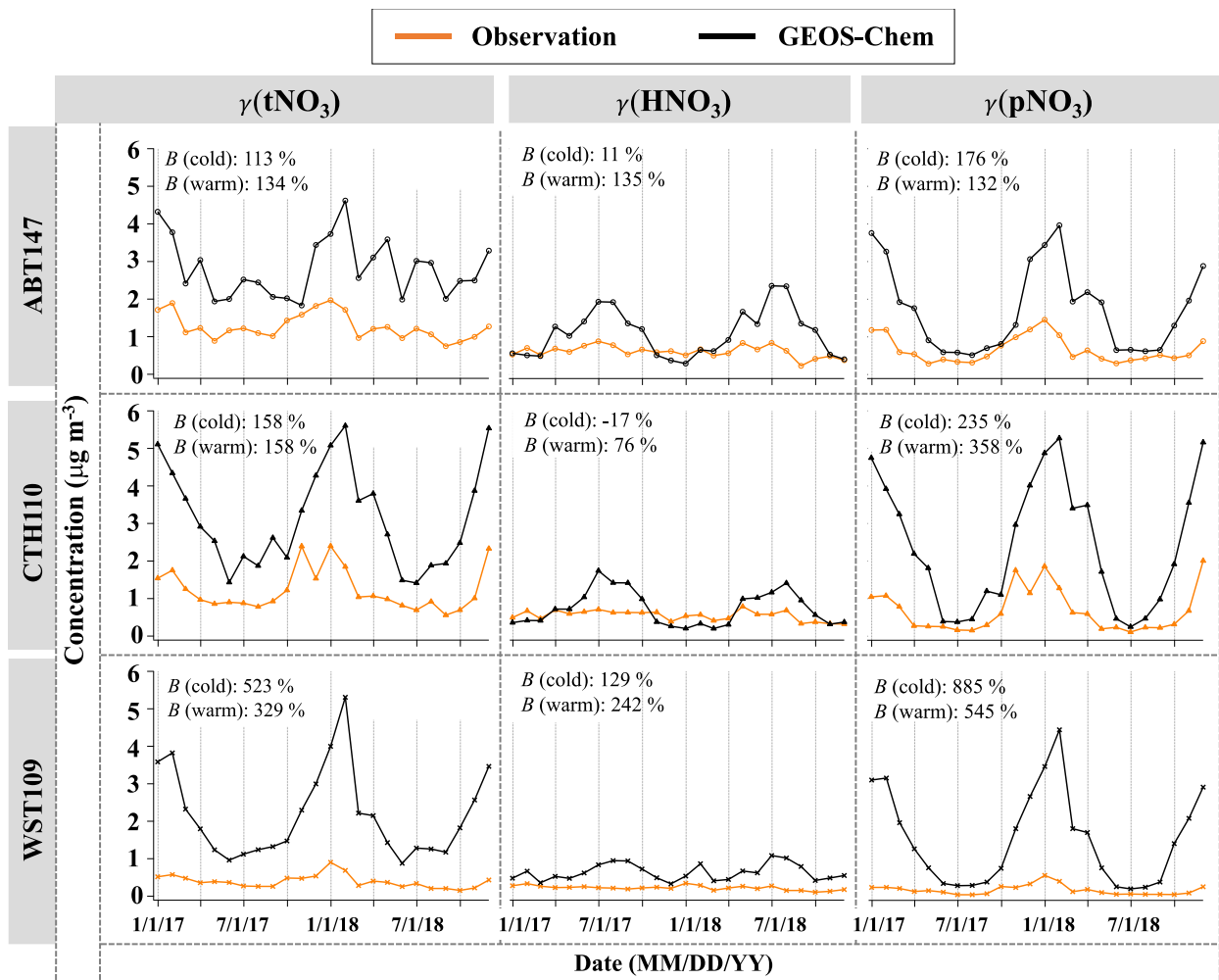
Figure 3. **Time series of monthly mean total nitrate, HNO₃, and pNO₃ concentrations (*γ*) observed and simulated at ABT147, CTH110, and WST109 CASTNET sites. *B* refers to the normalized mean bias for comparison of the model to observations (see section 2.3 in Methods).**

820
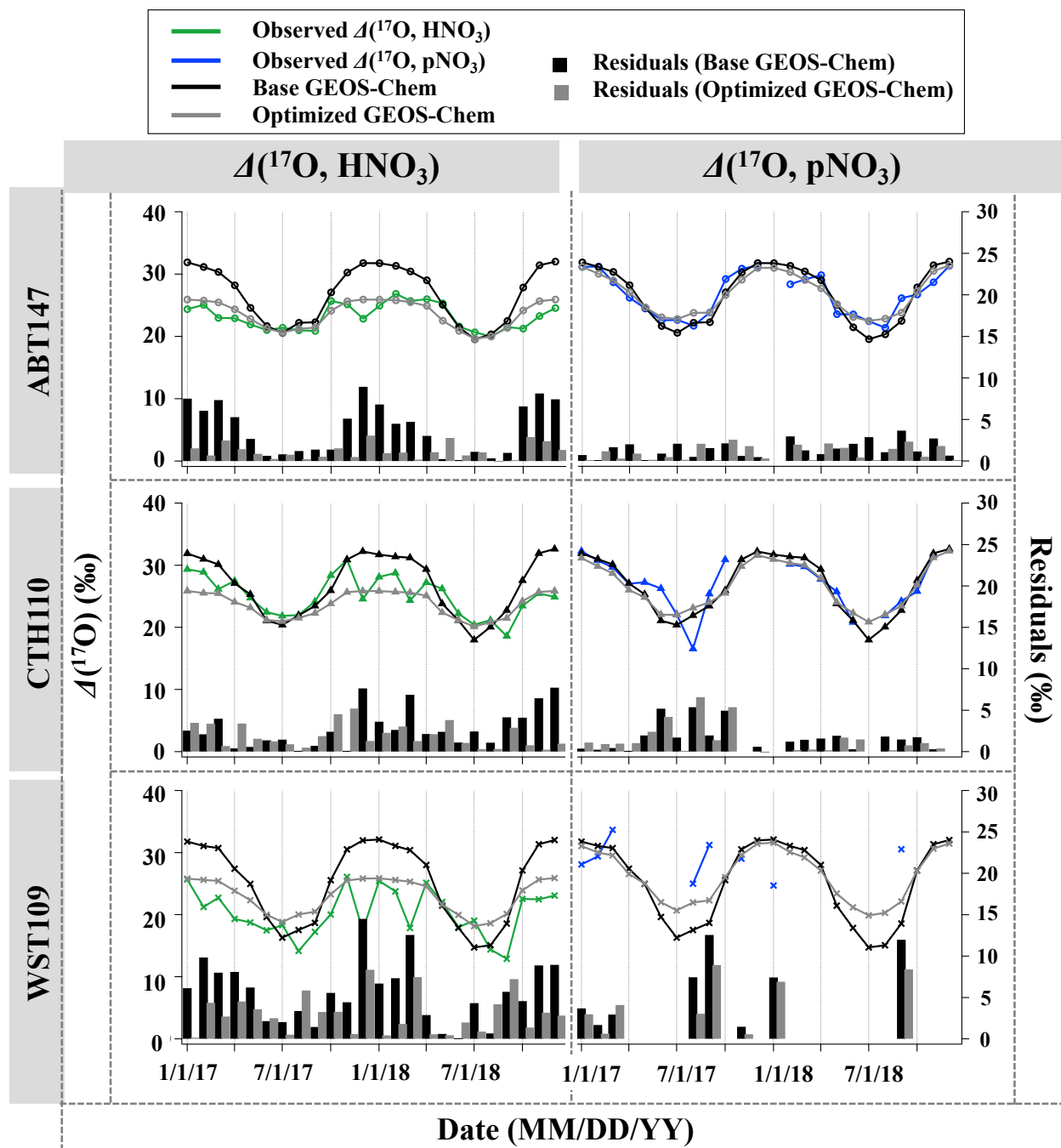
Figure 4. Time series of the monthly mean for observed and calculated $\Delta(^{17}O)$ for HNO₃ and pNO₃ over ABT147, CTH110, and WST109 CASTNET sites. Calculated $\Delta(^{17}O)$ using base (black) and optimized (grey) GEOS-Chem are shown in the plot together. Bars indicate the residuals between calculation and observation.

825
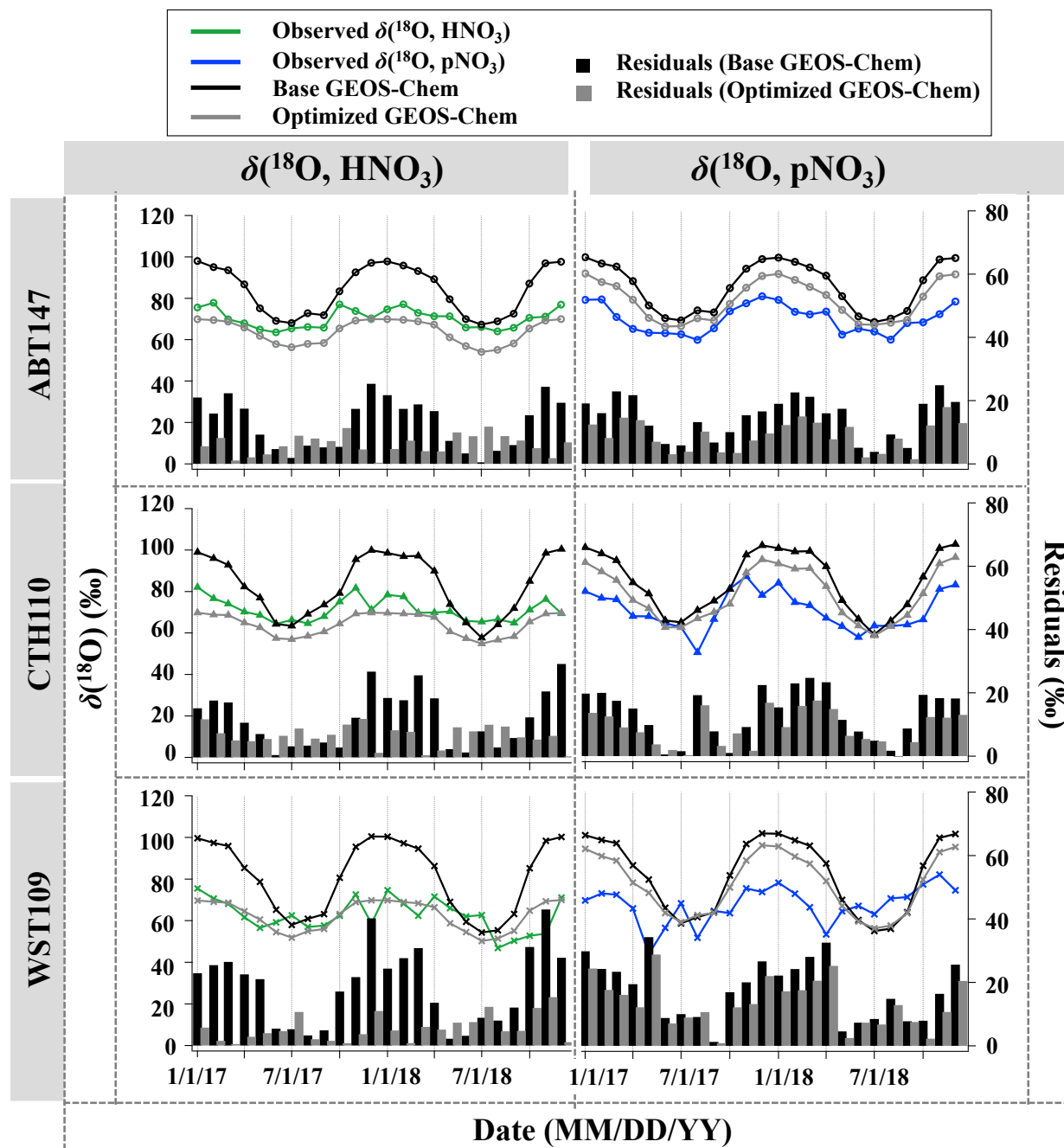
Figure 5. Time series of the monthly mean for observed and calculated $\delta(^{18}O)$ for HNO₃ and pNO₃ over ABT147, CTH110, and WST109 CASTNET sites. Calculated $\delta(^{18}O)$ using base (black) and optimized (grey) GEOS-Chem are shown in the plot together. Bars indicate the residuals between calculation and observation.
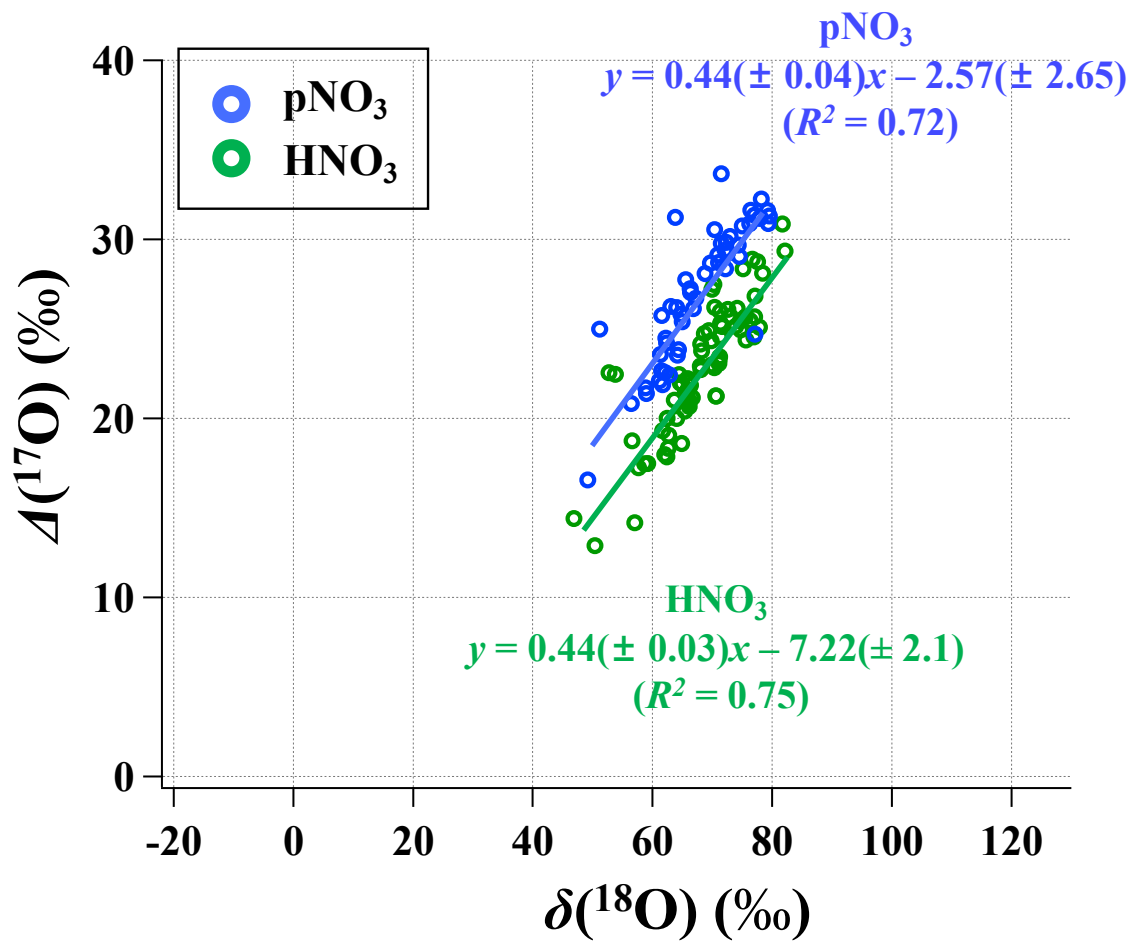
832

833 **Figure 6.** Relationship between the monthly mean ($\delta(^{18}O)$ and $\Delta(^{17}O)$) for observed HNO₃

834 **(green) and pNO₃ (blue) across all CASTNET sites with correlation coefficient (R^2) and slope**

835

836

837

838

839

840
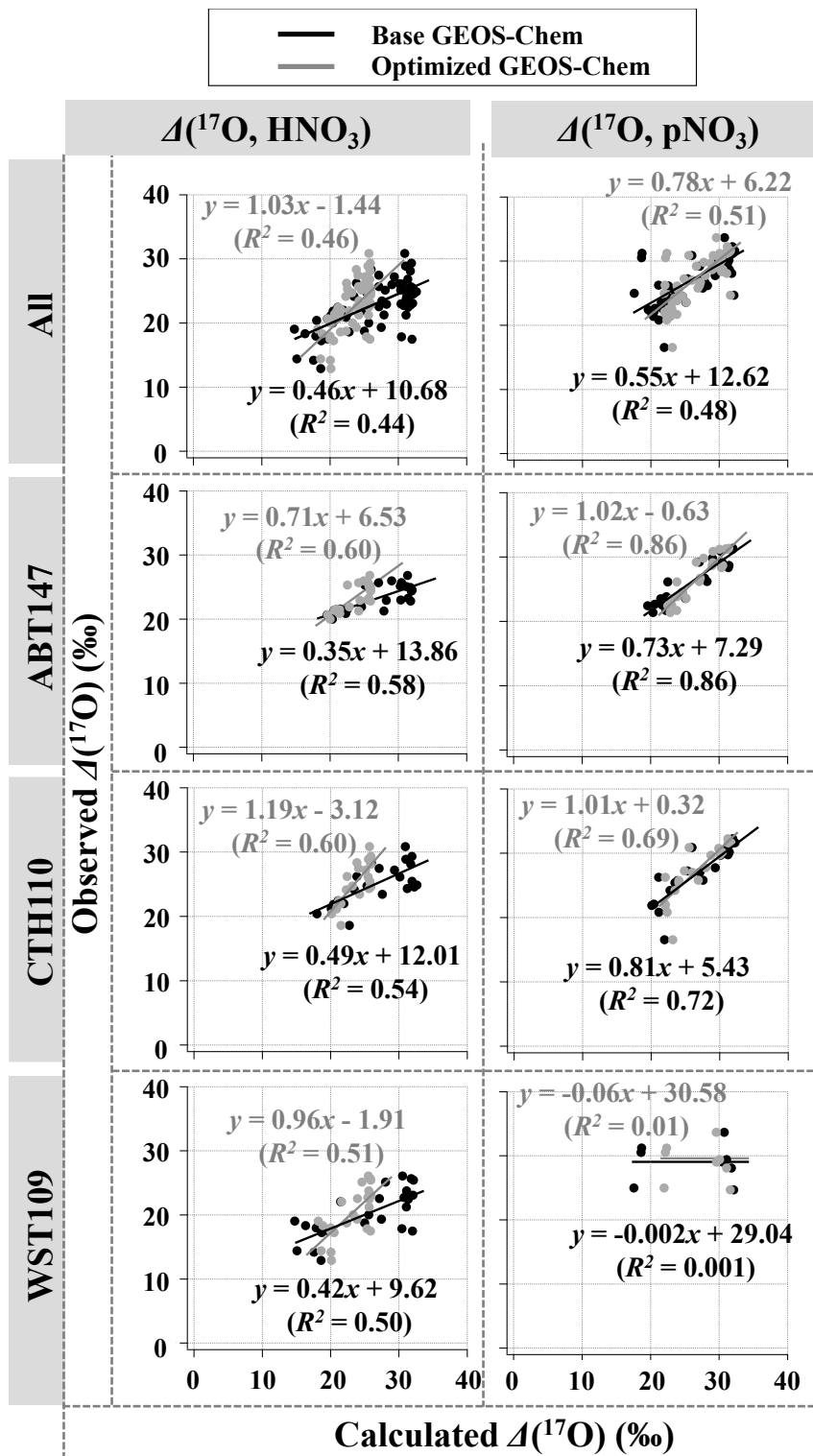
Figure 7. Correlation between observed and calculated $\Delta(^{17}O)$ for HNO_3 and pNO_3 using base GEOS-Chem (black) and optimized GEOS-Chem (grey) by each site.

845
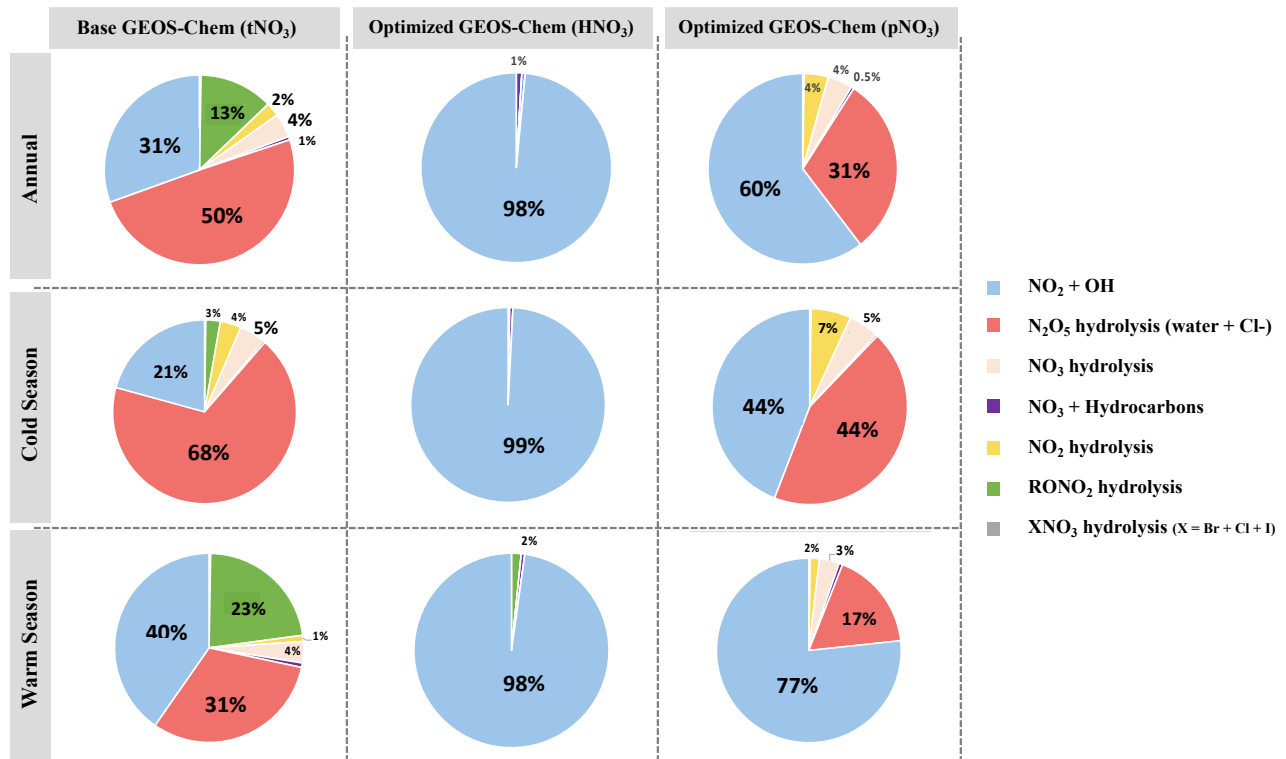
847 **Figure 8.** Relative proportions for major nitrate production pathways by season from base
848 **GEOS-Chem output (HNO₃ + pNO₃), optimized GEOS-Chem for HNO₃ production only,**
849 **and optimized GEOS-Chem for pNO₃ production only based on comparison with**
850 **observations across the three CASTNET sites. Annual refers to the full two-year record (Dec**
851 **2016-Dec 2018). The cold and warm seasons refer to Oct-Mar and Apr-Sep, respectively.**

852

853

854
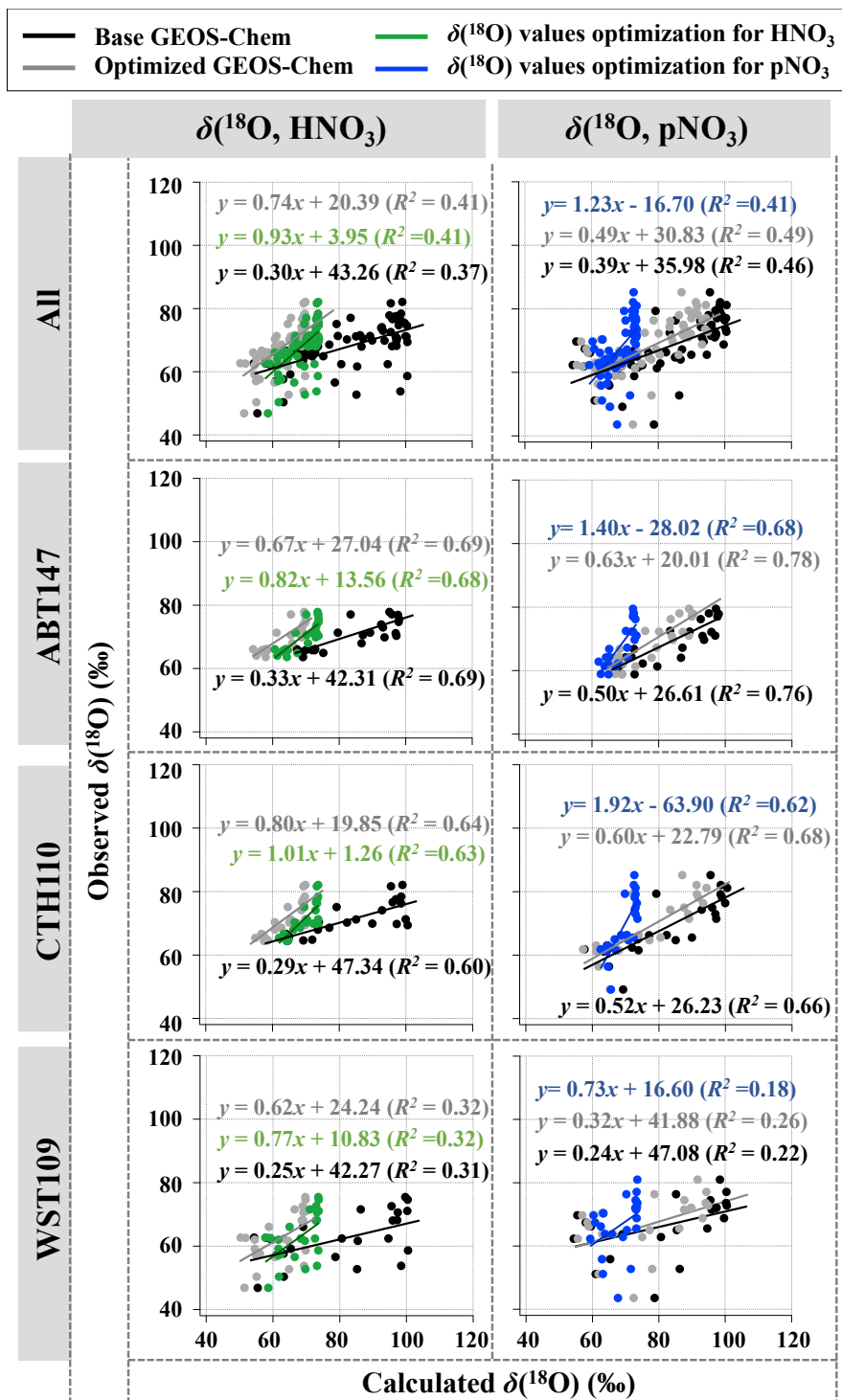
Figure 9. Correlation between observed and calculated $\delta(^{18}O)$ for HNO₃ and pNO₃ by each
site. Calculated $\delta(^{18}O)$ values using base GEOS-Chem, optimized GEOS-Chem, and
optimized $\delta(^{18}O)$ values indicated as black, grey, and green (for HNO₃) or blue (for pNO₃),
respectively.

859
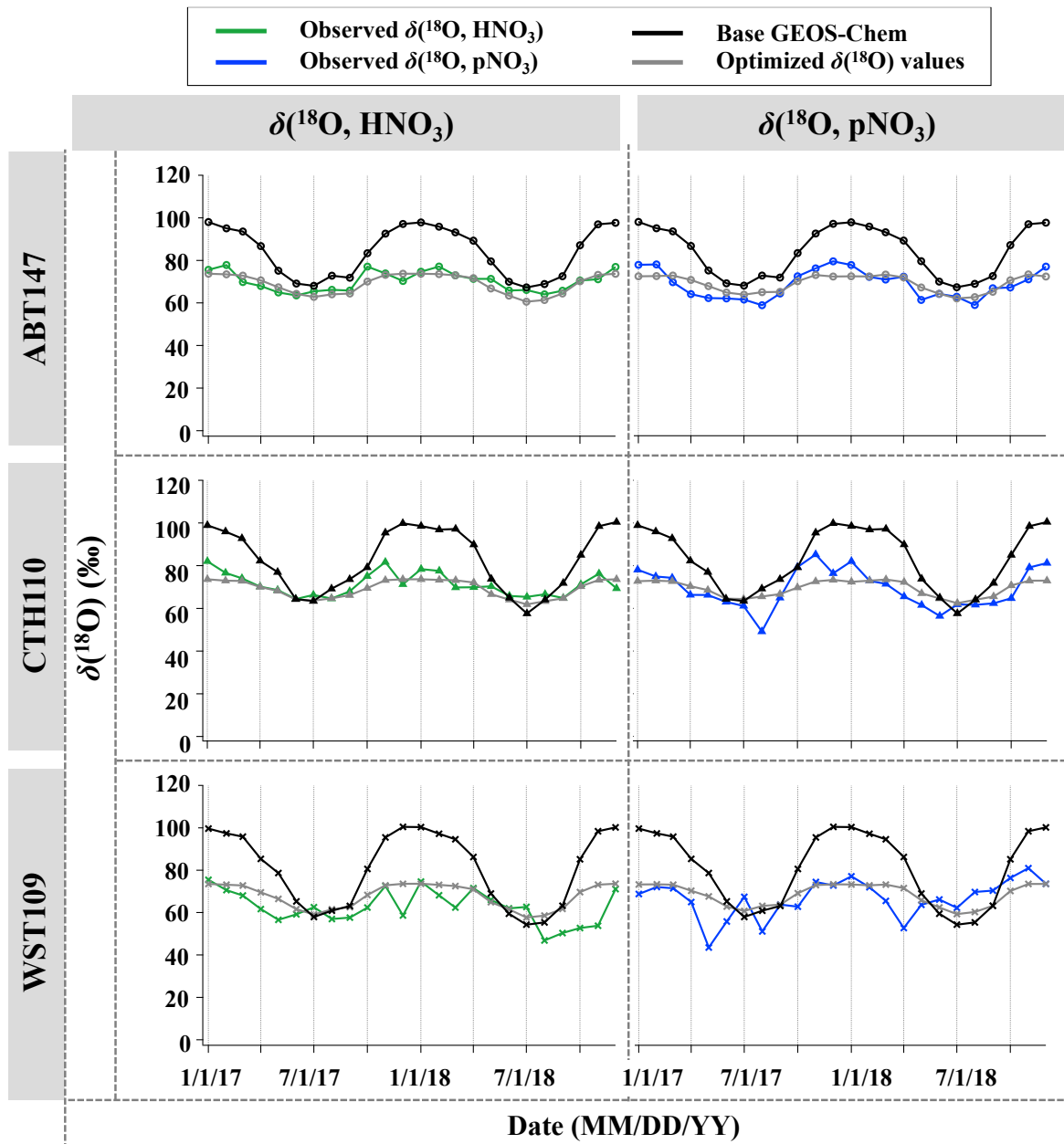
861 **Figure 10.** Time series of observed and calculated $\delta(^{18}O)$ for HNO₃ and pNO₃ for ABT147,

862 CTH110, and WST109 sites. Calculated $\delta(^{18}O)$ using base GEOS-Chem (black) and using

863 optimized $\delta(^{18}O)$ values (grey) are shown in the plot together.

864

865

866

Table 1. Equations for $\delta(^{18}O)$ and $\Delta(^{17}O)$ calculations by different nitrate formation pathways.

Gas-phase reactions	$\Delta(^{17}O, tNO_3)$	$\delta(^{18}O, tNO_3)$
$NO_2 + OH$	$\frac{2}{3}A\Delta(^{17}O, O_3{*})$	$\frac{2}{3}\delta(^{18}O, NO_2) + \frac{1}{3}\delta(^{18}O, OH)$
$NO_3 +$ Hydrocarbons	$(\frac{2}{3}A+\frac{1}{3})\Delta(^{17}O, O_3{*})$	$\frac{2}{3}\delta(^{18}O, NO_2) + \frac{1}{3}\delta(^{18}O, O_3{*})$
Heterogeneous reactions		
N_2O_5 hydrolysis (water + Cl$^-$)	$(\frac{2}{3}A+\frac{1}{6})\Delta(^{17}O, O_3{*})$	$\frac{4}{6}\delta(^{18}O, NO_2) + \frac{1}{6}\delta(^{18}O, O_3{*}) + \frac{1}{6}\delta(^{18}O, H_2O)$
NO_3 hydrolysis	$(\frac{2}{3}A+\frac{1}{3})\Delta(^{17}O, O_3{*})$	$\frac{2}{3}\delta(^{18}O, NO_2) + \frac{1}{3}\delta(^{18}O, O_3{*})$
NO_2 hydrolysis	$(\frac{2}{3}A+\frac{1}{3})\Delta(^{17}O, O_3{*})$	$\frac{2}{3}\delta(^{18}O, NO_2) + \frac{1}{3}\delta(^{18}O, H_2O)$
$RONO_2$ hydrolysis	$\frac{1}{3}A\,\Delta(^{17}O, O_3{*})$	$\frac{2}{3}\delta(^{18}O, NO_2) + \frac{1}{3}\delta(^{18}O, NO_2)$
XNO_3 hydrolysis (X = Br + Cl + I)	$(\frac{2}{3}A+\frac{1}{3})\Delta(^{17}O, O_3{*})$	$\frac{2}{3}\delta(^{18}O, NO_2) + \frac{1}{3}\delta(^{18}O, O_3{*})$

889 **Table 2.** Summary of the residuals between observed and calculated oxygen isotope deltas by
890 season using the base and optimized GEOS-Chem, respectively.

Residuals		$\Delta(^{17}O, HNO_3)$	$\Delta(^{17}O, pNO_3)$	$\delta(^{18}O, HNO_3)$	$\delta(^{18}O, pNO_3)$
Base GEOS-Chem	Annual	4.1 ‰	2.3 ‰	15.5 ‰	15.9 ‰
	Cold	6.2 ‰	1.7 ‰	23.1 ‰	20.4 ‰
	Warm	2.0 ‰	2.8 ‰	7.9 ‰	11.4 ‰
Optimized GEOS-Chem	Annual	2.0 ‰	1.7 ‰	6.2 ‰	10.4 ‰
	Cold	2.3 ‰	1.4 ‰	5.7 ‰	13.2 ‰
	Warm	1.8 ‰	2.0 ‰	6.7 ‰	7.7 ‰

891
892
893
894
895
896
897
898
899
900
901
902
903
904
905
906
907
908
909
910
911
912
913

914 **Table 3.** $\delta(^{18}O)$ **values for each oxidant before and after optimization based on different**

915 **scenarios**

Atmospheric Oxidants	Assumed $\delta^{18}O$ (‰)	Optimized $\delta^{18}O$ (‰)			
		Non-fixed	Fixed O_3^*	Fixed O_3^* and H_2O	Fixed O_3^*, H_2O, and O_2
O_3^*	126.3	89.9	-	-	-
H_2O	-6.0	-6.5	-180.7	-	-
$O_2/RO_2/HO_2$	23.0	11.1	40.9	44.4	-
OH	-43.0	42.2	-31.3	-39.4	-36

916

917